UNIVERSITÄTSKLINIKUM HAMBURG-EPPENDORF

Zentrum für Experimentelle Medizin, Institut für Tumorbiologie

Direktor: Prof. Dr. med. Klaus Pantel

Exosomal microRNAs as tumor markers in epithelial ovarian cancer

Dissertation

zur Erlangung des Grades eines Doktors der Medizin /Zahnmedizin
an der Medizinischen Fakultät der Universität Hamburg.

vorgelegt von:

Chi Pan

aus Jiangsu (China)

Hamburg 2018

(wird von der Medizinischen Fakultät ausgefüllt)

Angenommen von der
Medizinischen Fakultät der Universität Hamburg am: 04.10.2018

Veröffentlicht mit Genehmigung der
Medizinischen Fakultät der Universität Hamburg.

Prüfungsausschuss, der/die Vorsitzende:

Prüfungsausschuss, zweite/r Gutachter/in:

II

CONTENTS

1. Introduction

1.1. Ovarian cancer

In the female reproductive system, ovarian cancer is one of the most aggressive carcinomas and the leading cause of death among gynecologic malignancies because of its frequent recurrence and resistance to chemotherapy. Most women fall sick between the ages of 60 and 65. Ovarian cancer develops asymptomatically at early stages and therefore is recognized lately, so that the patients have a poor prognosis. More than two-thirds of patients are diagnosed at advanced FIGO (International Federation of Gynecology and Obstetrics) stages III or IV and have a 5-year survival rate of less than 40% than patients who are diagnosed with FIGO stage I or II and have a longer 5-year survival rate of around 80% (1).

1.1.1. Histological subtypes of ovarian cancer

Ovarian cancer is mainly a primary tumor arising from germ cells, stromal tissue, or epithelial tissue within the ovary. About 7% of ovarian cancers are of secondary origin, resulting of metastasis from a primary cancer in another organ (e.g., breast, colon, appendix, and stomach) (2). Epithelial ovarian cancer (EOC) is the most common subtype (approximately 95%) of ovarian cancer. Non-epithelial histotypes, including germ cell tumors and stromal tumors are very rare in ovarian cancer (3). EOC is a heterogeneous disease commonly classified into five major histological subtypes of invasive disease: high grade serous ovarian carcinoma (HGSOC), low grade serous ovarian carcinoma (LGSOC), mucinous ovarian carcinoma (MOC), endometrioid ovarian carcinoma (ENOC) and clear cell ovarian carcinoma (CCOC) (4, 5). There is also another classification of EOC into two different tumor types: Type I and Type II (Figure 1.1.). Type I tumors include LGSOC, low grade endometrioid ovarian carcinoma (LGEOC), MOC, and a subset of CCOC. These tumors develop slowly and are normally confined to the ovary. In contrast, Type II tumors include HGSOC, undifferentiated carcinoma, malignant mixed mesodermal tumor (carcinosarcoma), and some

CCOC. According to their high grade and quick growth, they generally spread beyond the ovary at the time of diagnosis (6). These tumors are inherently different diseases, due to their differences in epidemiological and genetic risk factors, precursor lesions, patterns of spread, molecular events during oncogenesis, response to chemotherapy, and prognosis (7).
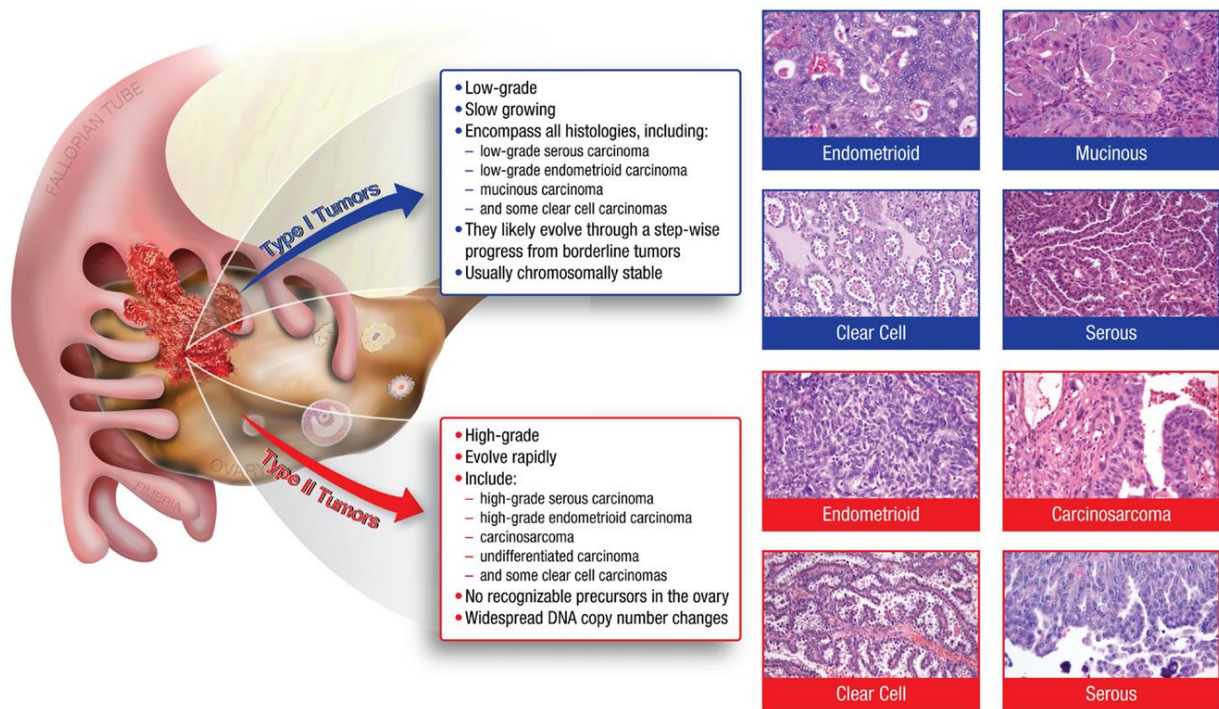
Figure 1.1. Two tumor types of EOC (from Paul Michael Jones and Ronny Drapkin, Front Oncol, 2013)

Type I tumors are low-grade, slow growing carcinomas that typically arise from well recognized precursors lesions (borderline tumors) and develop from the ovarian surface epithelium, inclusion cysts, or endometriosis. Type II tumors are high-grade and rapidly growing carcinomas. These tumors progress rapidly, harbor TP53 mutations, and exhibit widespread DNA copy number alterations.

1.1.2. FIGO staging classification of ovarian cancer

FIGO staging classification of ovarian cancer is according to National Comprehensive Cancer Network (NCCN) Guidelines Version 1.2016 and as followed:

FIGO I. Tumor confined to ovaries or fallopian tube(s).

FIGO II. Tumor involves one or both ovaries or fallopian tubes with pelvic extension (below pelvic brim) or primary peritoneal cancer.

2

FIGO III. Tumor involves one or both ovaries or fallopian tubes, or primary peritoneal cancer, with cytologically or histologically confirmed spread to the peritoneum outside the pelvis and/or metastasis to the retroperitoneal lymph nodes.

FIGO IV. Distant metastasis excluding peritoneal metastases.

1.1.3. Cancer grades for ovarian cancer

Ovarian cancer is classified into three grades according to its cell differentiation as determined by pathologists: Grade 1, Grade 2 and Grade 3. Grade 1 includes ovarian cancer cells that are well-differentiated, similar to healthy ovarian tissue and have lower possibility to metastasize. Grade 1 is also called low grade. Grade 2 includes ovarian cancer cells that are moderately-differentiated. Ovarian cancer cells of Grade 3 are poorly-differentiated, more irregular and have more potential to metastasize. Thus, Grade 3 is also called high grade. Therefore, the lower the grade, the slower the cancer cells proliferate.

1.1.4. Metastasis of ovarian cancer

Ovarian cancer metastasizes early by direct extension from the ovarian/fallopian tumor to neighboring organs (bladder/colon) (8). Typically, tumor cells begin to metastasize by growing in the peritoneal cavity (2). Peritoneal seeding is the most common pathway for the spread of ovarian cancer, so that at diagnosis nearly two thirds of ovarian cancer patients have already developed peritoneal metastasis (9). Unlike most other cancers, ovarian cancer rarely disseminates through the vasculature (8). However, ovarian cancer cells can travel through the lymphatic system and metastasize to lymph nodes connected to the ovaries via blood vessels (10). Ovarian cancer cells, often forming cellular aggregates or spheroids, are then transported throughout the peritoneal cavity and subsequently implant on the peritoneal wall, gastrointestinal tract, omentum, and diaphragm (11). Figure 1.2 illustrates a model for intraperitoneal dissemination of ovarian cancer.
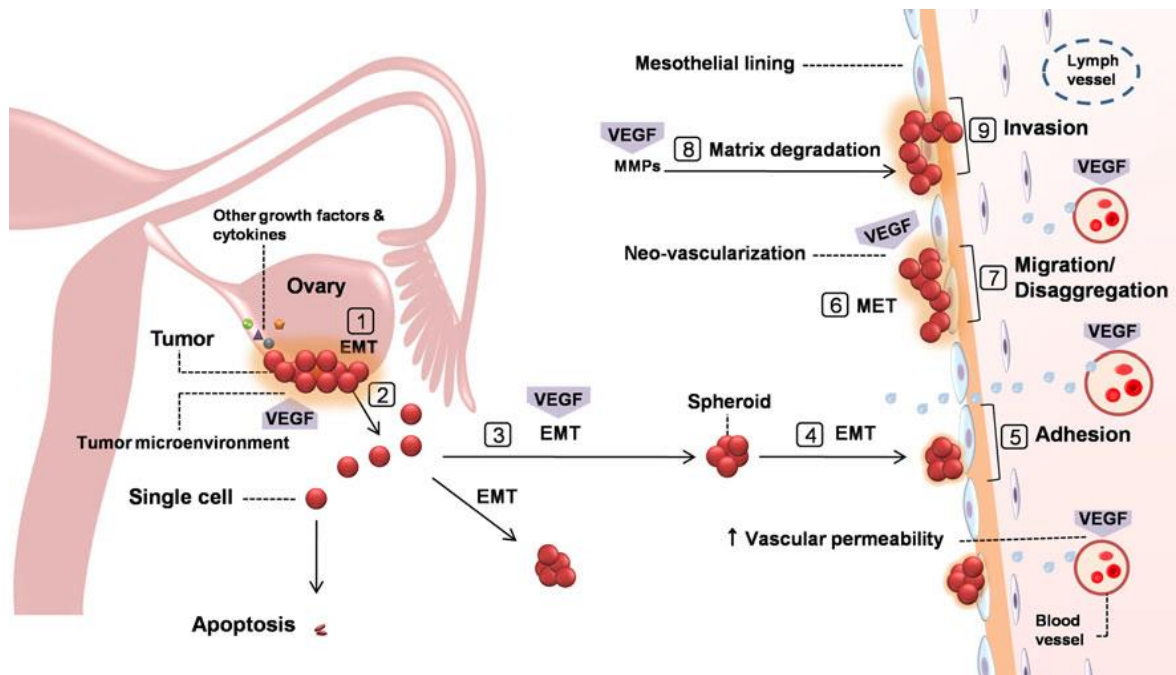
Figure 1.2. A proposed model for intraperitoneal dissemination of ovarian cancer (from Moghaddam et al., Cancer Metastasis Rev, 2012)

Primary tumors undergo epithelial-mesenchymal transition (EMT) to metastasize **(1)**. Then, ruptured tumor sheds its cancer cells into the peritoneum **(2)**, where they often form spheroids to survive **(3)**. Spheroids EMT into invasive mesenchymal phenotype to maintain survival and motility **(4)**. These cells are transported throughout the peritoneal cavity by normal peritoneal fluid and then adhere to and implant on the peritoneum and mesothelial linings of pelvic and abdominal organs **(5)**, where they undergo mesenchymal-epithelial transition (MET) **(6)** and disaggregation **(7)** to initiate metastatic growth. Through the activity of matrix metalloproteinases (MMPs), matrix degradation occurs **(8)**, and cancer cells infiltrate the mesothelial lining and the extracellular matrix **(9)**. In the entire process, vascular endothelial growth factor (VEGF) is involved in primary tumor angiogenesis, neovascularization at newly seeded sites, MMP-mediated matrix degradation, and malignant ascites formation.

1.1.5. Symptom and diagnosis of ovarian cancer

There are no specific methods for screening and detection of early ovarian cancer. With the increase of tumor size, patients feel abdominal falling, bloating and other minor discomfort in

the abdomen. Ascites usually floods in the abdominal cavity in advanced ovarian cancer. At late stages, the rapid swelling of abdomen may cause some symptoms, such as the air choke, weight loss and fever. There are also symptoms caused by complications of ovarian tumors, like tumor torsion, rupture and infection, which in turn may cause acute abdominal pain, fever and even shock.

The tumor marker CA125 (Carbohydrate Antigen 125) is expressed in most high-grade serous carcinoma, but only in 60% of mucinous and clear cell subtypes (12). Thus, a blood test measuring changes in CA125 concentrations is highly effective in detecting late stage ovarian cancer. However, CA125 measurements are not sufficiently sensitive to diagnose EOC at an early stage, since only ~40% of patients with invasive epithelial ovarian or tubal cancer are detected at stage I or II (13). Normally, CA-125 levels of less than 35 U/ml are accepted as normal (14, 15), as well as 35-65 U/ml and >65 U/ml are considered as threshold and abnormal, respectively (16, 17). However CA125 not only rises in ovarian cancer, but also in endometriosis, and pelvic inflammatory (18). Transvaginal ultrasound is used as a second-line test in ovarian cancer (19). In addition, pelvic examination, computed tomography, X-ray and magnetic resonance imaging (MRI) are applied.

1.1.6. Treatment of ovarian cancer

The standard treatment for ovarian cancer is maximal cytoreductive surgical debulking followed by a first-line chemotherapy (intravenous platinum/taxane regimes). Determination of staging of the disease is very important before chemotherapy, and also performed during surgery. The histological type of the tumor, including grading should be defined. High-grade/low-grade scale is currently used, except for endometrioid ovarian cancer where a three-grade scale is used (G1, G2 or G3). Staging assessment in surgical-pathologic degrees should be done according to current FIGO recommendations (20). Advanced ovarian cancer standard treatment involves surgical resection and chemotherapy with carboplatin and paclitaxel. Despite high proportions of patients achieving a response with standard first-line chemotherapy, most women relapse (21). Treatment for initial recurrent disease depends on many factors, such as duration of initial treatment response, antecedent

and persistent adverse events, performance status, histology, location and burden of disease, and genetic alterations (e.g., BRCA mutation status) (22). A second-line chemotherapy is recommended for most patients who develop recurrence. Because most recurrent tumors are platinum sensitive, a combined treatment of platinum-containing regiments can be applied (1).

1.2. Ovarian benign tumors

Of all ovarian tumors, 90% are benign, although this varies with age (23). Ovarian serous cystadenoma, a type of benign ovarian epithelial tumor, accounts for about 60% of ovarian serous tumors (24). Generally, it is asymptomatic and does not recur following oophorectomy.

Ovarian mucinous cystadenoma is a type of cystic adenoma, and accounts for 15% in all benign ovarian neoplasms (25). It normally occurs in women aged from twenties to forties, but also in adolescent and premenarchal girls (26). This tumor type originates from the fluid or mucus. Likely serous cystadenoma, patients with this disease do not have any symptoms. However, when tumors turn malignant, they can grow to be extremely large and cause abdominal pain and distension in patients (27). After surgical treatment, the recurrence of this tumor is very rare.

Other ovarian benign tumors, such as ovarian cystadenofibroma is relatively uncommon, and it accounts approximately 1.7 % of all benign ovarian tumors (28). Sclerosing stromal tumor is a rare ovarian neoplasm and normally included in the fibroma-thecoma group of ovarian tumors (29).

1.3. Exosomes

1.3.1. Exosome biogenesis

Exosomes are microvesicles ranging from approximately 30 to 100 nm in size, and are secreted by all living cells under normal and pathological conditions (30, 31). They can be found in most body fluids, including blood, saliva, ascites and urine. For identification of

exosomes, CD9, CD63, CD81 and CD82 are classically used as exosome markers (32, 33). The biogenesis of exosomes starts with the endocytosis of microvesicles to produce an early sorting endosome. A part of early sorting endosomes recycle to endosomes or lysosomes. The others of early sorting endosomes mature into multivesicular bodies (MVBs). Then, MBVs are packaged with genetic materials and proteins. Some late MVBs fuse with lysosomes, and the others fuse with the plasma membrane and are released as exosomes into the extracellular space. Exosomes deliver their cargo, such as microRNAs (miRNAs), to the recipient cell by fusing with its cell membrane to induce cell-to-cell communications (Figure 1.3.) (34).
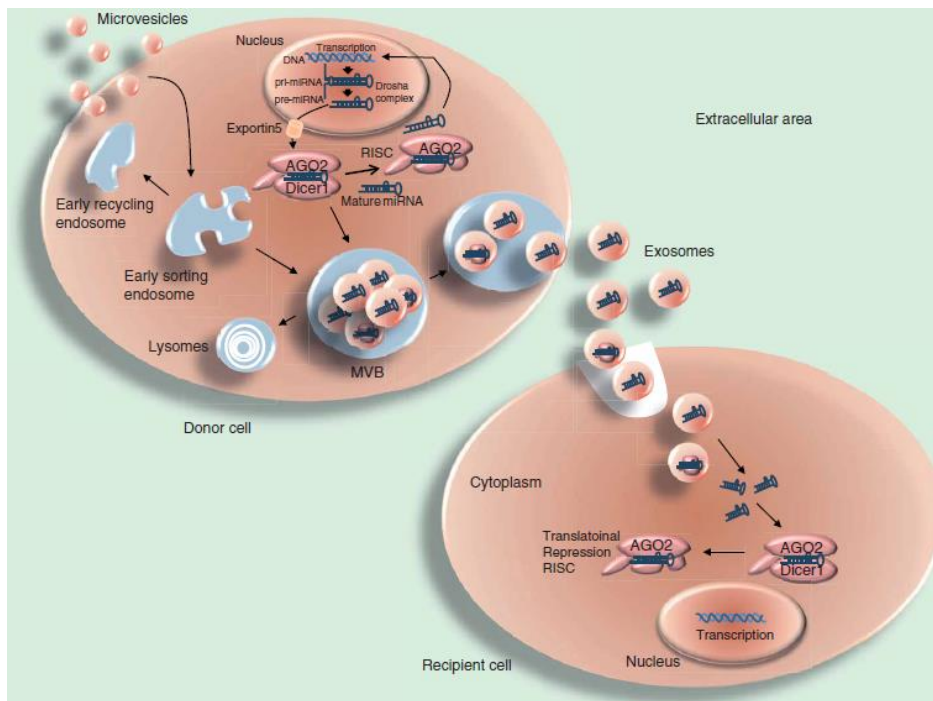
Figure 1.3. Biogenesis and cell-to-cell communications of exosomes (from Schwarzenbach, Expert Rev Mol Diagn, 2015)

The endocytosis of microvesicles produce early endosomes, and some early endosomes mature to MVBs. The late MVBs packaged with genetic materials and proteins are released as exosomes into extracellular space and uptaken by the recipient cell. There, the exosomes release their content, e.g., miRNAs. MiRNAs are functionally active by binding to their target mRNA in the miRNA-induced silencing complex (RISC) to repress the translation of the mRNA into protein. This can result in changes of the characteristics of the recipient cell.

1.3.2. Exosome function

Exosomes are protected by a lipid bilayer, which enables them to carry genetic information to distant sites through the bloodstream (35). Increased secretion of exosomes has been associated with tumor invasiveness both in vitro and in vivo, and to promote migration and proliferation of tumor cells leading to metastasis (36). It has been reported that concentrations of exosomes in the serum of EOC patients were higher than those of healthy women (17). Exosomes can also serve as mediators for intercellular communication through the delivery of their cargo, including protein, lipids, nucleic acids (miRNAs, mRNAs and DNAs) or other cellular components, to neighboring or distant cells (37). Cancer-derived exosomes may mediate propagation of cancer by transferring pathogenic factors from cancer to healthy cells (38, 39). Thus, discharging of the exosome contents in the recipient cells can alter the fate of these cells. Since exosomes can cover wide distances, they can also influence distantly located cells and tissues. The process of sorting and packaging of miRNAs into exosomes seems to be selective, favoring certain miRNAs for exosomal transfer over others (34, 40).

1.4. MiRNAs

1.4.1. MiRNAs biogenesis

MiRNAs are a family of evolutionary conserved, small non-coding RNA molecules consisting of approximately 22 nucleotides encoded by the genome of vertebrates, invertebrates and plants. MiRNAs are released inactively by apoptotic or necrotic cells, and actively by exosomes. In the canonical pathway, the primary miRNA (pri-miRNA) is transcribed from genome. Then, the pri-miRNA is cleaved by the Drosha complex (RNase III type endonuclease) into the precursor miRNA (pre-miRNA) of ~70 nucleotides in length. With the assistance of the RNA-binding protein TRBP (tar-RNA binding protein), Dicer, a multi-domain RNase III-type protein, processes pre-miRNA to generate a ~20-bp miRNA-miRNA duplex. One strand of the duplex is the mature miRNA. It is bound to the AGO2 protein and

integrated in the RISC complex. The other strand of the duplex is released and degraded or also loaded into the RISC complex, to function as a mature miRNA (Figure 1.4.) (41).
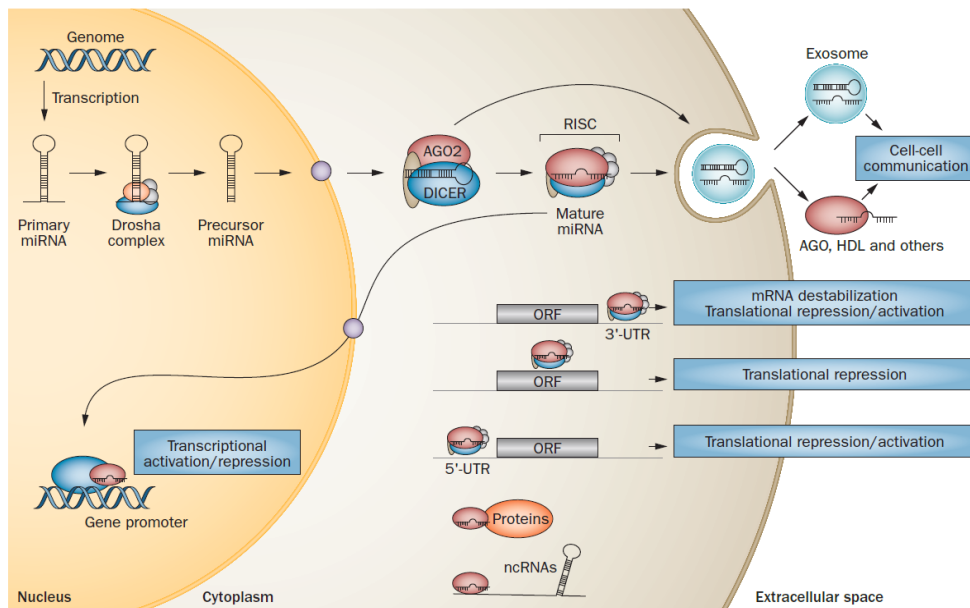
Figure 1.4. Biogenesis and functions of miRNAs (from Schwarzenbach et al., Nat Rev Clin Oncol, 2014)

Pri-miRNAs are originally transcribed from RNA polymerase II (RNAPII)-specific transcripts of independent genes or from introns of protein-coding genes. In the canonical pathway, pri-miRNAs are cleaved by the Drosha complex and processed as 70-nucleotide stem loop pre-miRNAs. After being exported from the nucleus to the cytoplasm by Exportin 5 protein, pre-miRNAs are then processed by DICER, an RNase III type endonuclease, forming mature miRNAs. One strand of the double-strand mature miRNAs is loaded into the RISC complex, containing the AGO family protein as a core component. In the RISC complex, mature miRNAs bind to the 3'untranslated-region (UTR) of their target mRNA, and repress its translation or destabilize the mRNA. MiRNAs have also the ability to bind to the open reading frame (ORF) and the 5'-UTR of the target mRNA, activating or repressing its translational efficiency.

1.4.2. MiRNAs functions

MiRNAs play an important part in many cellular processes, such as differentiation, proliferation, apoptosis, and stress response. Additionally, they are key regulators in many

diseases, such as benign diseases, vascular diseases, viral infection, and cancer (42). In cytoplasm, they bind to the 3´-UTR of their target mRNAs and inhibit protein synthesis by either repressing translation or promoting mRNA destabilization (43). A core sequence of only 2–7 nucleotides is necessary for their binding. In most cases, miRNAs only partly bind to their complementary target mRNA sequence (44). When RISC containing AGO2 in mammals encounters mRNAs bearing sites nearly perfectly complementary to miRNA, these mRNAs are cleaved and degraded witch leading to gene silencing (45). MiRNAs have also the ability to bind to the ORF and the 5'-UTR of the target mRNA, activating or repressing its translational efficiency. Moreover, they can function dually as an oncogene and tumor-suppressor gene depending on the cancer type and cellular context (46). Computational analyses indicate that one miRNA has binding affinity to hundreds of different mRNAs and hence, miRNAs regulate numerous signal transduction pathways involved in development, differentiation, proliferation and tumor development and progression (47).

2. Material and Methods

2.1. Patients

Blood samples were collected from 106 ovarian cancer patients directly before surgery from September 2009 to October 2015. The patients were treated according to national guidelines at the University Medical Center Hamburg-Eppendorf, Department of Gynecology, and histologically confirmed for FIGO stages I-IV. In addition, 8 plasma samples from ovarian cystadenoma patients and 29 plasma samples from healthy women who had no history of cancer and were in good health based on self-report. Blood samples of patients with ovarian cystadenoma and healthy women were obtained from May 2017 to June 2017 and during 2015–2016, respectively. Blood collection and experiments were performed in compliance with the Helsinki Declaration and were approved by the ethics committee (Ethik-Kommission der Ärztekammer Hamburg, Hamburg). Regarding blood processing, uniform management concerning the specific, described protocols was performed. Detailed patient characteristics are summarized in Table 1.3.1.1.

2.2. Cell lines

For functional analyses, ovarian cancer cell lines SKOV3 and OVCAR3 purchased from American Type Culture Collection (ATCC) were used. Cell lines SKOV3 and OVCAR3 were authenticated by the Leibniz Institute Deutsche Sammlung von Mikroorganismen und Zellkulturen GmbH (DSMZ), Braunschweig, on 14/06/2013 and 30/07/2013. Aliquots were frozen in liquid nitrogen and a new aliquot of these cell lines were used for this study. SKOV3 and OVCAR3 were cultured in McCoy's 5A modified medium and RPMI 1640, respectively, supplemented with 10% FCS (fetal calf serum; PAA, Laboratories, Cölbe, Germany) and 100 U/ml penicillin and streptomycin under standard conditions (37°C, 5% CO_2, humidified atmosphere). Cell lines were regularly tested for mycoplasma contamination.

2.3 Verification of hemolysis in plasma samples

To avoid quantifying exosomal miRNAs in hemolytic plasma samples that may influence the results, I performed hemoglobin measurements by spectral analysis. In 7 ml of whole blood red blood cells were lysed by erythrocyte lysis buffer (containing 0.3 M sucrose, 10 mM Tris pH 7.5, 5 mM $MgCl_2$ and 1% Triton X100). A dilution series (1:1, 1:3, 1:4, 1:6, 1:8, 1:10, 1:12, 1:14, 1:18, 1:20) of lysed red blood cells in plasma was prepared that served as a standard curve for the measurement of hemolysis in all plasma samples. Fifty µl of each plasma sample (standard and plasma of interest) were measured in duplicates on a Microplate reader (Tecan, Männerdorf, Switzerland). Absorbance peaks at 414, 541 and 576 nm were indicative for free hemoglobin, with the highest peak at 414 nm. The higher the absorbance in samples is the higher is the degree of hemolysis. The average values and standard deviations were calculated from the duplicates (Figure 2.1).

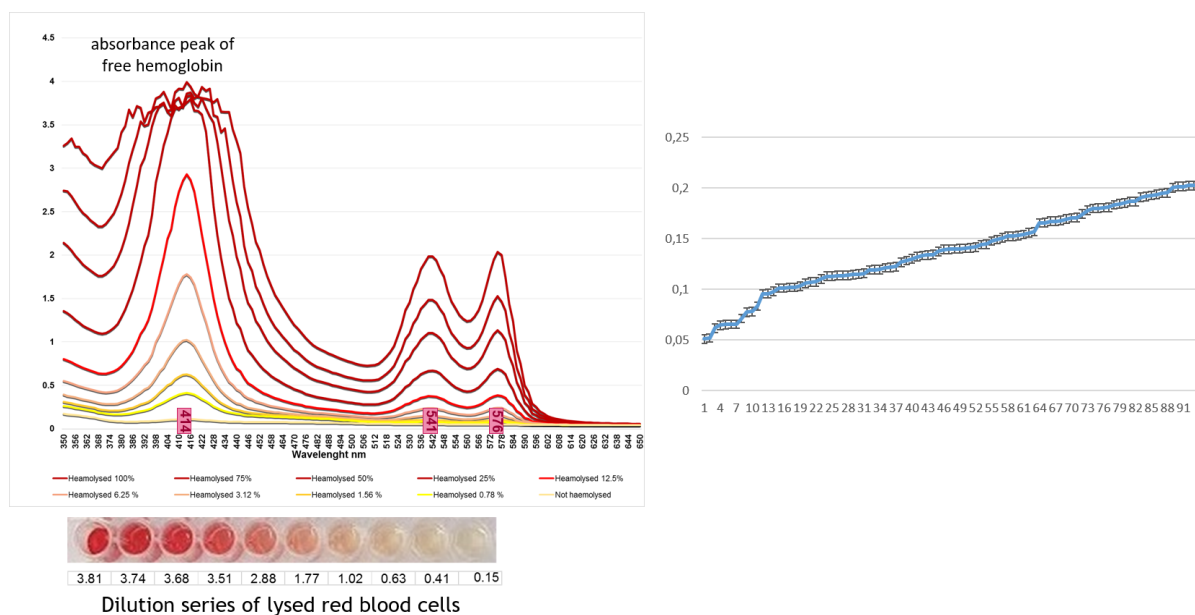**Figure 2.1. Levels of free hemoglobin measured in the plasma samples**

Hemolysis was assessed by spectrophotometry at wavelengths from 350 to 650 nm. A dilution series of lysed red blood cells in plasma was prepared (below the chart). The degree of hemolysis was determined based on the optical density (OD) at 414 nm (absorbance peak of free hemoglobin, called Soret band), with additional peaks at 541 and 576 nm. Samples

were classified as being hemolysed if the OD at 414 exceeded over 0.25. The integrated curve of plasma samples comprises values from 0.05 to 0.20 indicating that the samples were non-hemolysed.

2.4. Isolation of total exosomes from plasma

Plasma was prepared by 3 centrifugations steps at 300 g for 10 min, 2000 g for 10 min and 10 000 g for 30 min to remove cells and cell debris. Exosomes were then isolated from 143 plasma samples by ExoQuick (BioCat, Heidelberg, Germany) according to the manufacturer's instructions. Briefly, 500 µl of plasma were incubated with 120 µl ExoQuick exosome precipitation solution at 4 °C for 30 min. The plasma-ExoQuick mixture was centrifuged at 1,500 × g for 30 min and then, the supernatant was removed. Following an additional centrifugation at 1,500 g for 5 min, to remove residual fluid, the precipitated exosomes were then resuspended in PBS (Phosphate-Buffered Saline) buffer (Life Technologies, Darmstadt, Germany).

2.5. Extraction of miRNAs and conversion into cDNA

Exosomes were resuspended in 150 µl lysis buffer from the TaqMan microRNA ABC Purification Kit A (Thermo Fisher Scientific, Darmstadt, Germany). Eighty µl beads (TaqMan™ miRNA ABC Purification Bead kit Human panel A, Thermo Fisher Scientific) bound by a unique set of 377 anti-miRNA oligonucleotides were added to lysed exosomes to capture the specific miRNAs. For extraction efficiency, 2 µl of 1 nM synthetic cel-miR-39 were added as an exogenous spike in control. The beads with the extracted miRNAs were washed by 100 µl wash buffer 1 and 2 to remove DNA, proteins, contaminants, and residual binding solution (Thermo Fisher Scientific). The captured miRNAs were then eluted from the beads in 20 µl of elution buffer (Thermo Fisher Scientific). The extracted miRNAs were immediately reverse transcribed into cDNA (complementary DNA) using a modified protocol of TaqMan MicroRNA Reverse Transcription kit (Thermo Fisher Scientific) and on a MJ Research PTC-200 Peltier Thermal Cycler (Global Medical Instrumentation, Ramsey,

Minnesota, USA). Details of the RT-PCR (reverse transcription-polymerase chain reaction) are as followed:

Components	Volume (µl) for exosomal miRNAs
Custom RT primer pool	6
100mM dNTPs	0.3
MultiScribe Reverse Transcriptase (50 U/µl)	3
10x Reverse Transcription Buffer	1.5
RNase Inhibitor (20 U/µl)	0.19
RNA	4

PCR program

Temperature	Time
16 °C	30 min
42 °C	30 min
85 °C	5 min
4 °C	~

2.6. Preamplification of cDNA

Because of the low expression levels of exosomal miRNAs in the plasma of EOC patients, patients with ovarian cystadenoma and healthy women, and therefore, to increase the input cDNA, a preamplification step of cDNA was included. Five µl cDNA were preamplified in a 25-µl reaction containing 12.5 µl TaqMan PreAmp Master Mix and 3.75 µl Custom PreAmp Primer Pool (Thermo Fisher Scientific). To avoid false positive data (e.g., primer dimer formation or unspecific PCR products), a negative control without any templates was included from the starting point of reverse transcription. PCR was run on a MJ Research PTC-200 Peltier Thermal Cycler (Global Medical Instrumentation). Preamplification was carried out as followed:

Components	Volume (µl) for exosomal miRNAs
TaqMan PreAmp Master Mix	12.5
Custom PreAmp Primer Pool	3.75

Nuclease-free Water	3.75
cDNA	5

PCR program

Temperature	Time	
95 °C	10 min	
55 °C	2 min	
72 °C	2 min	
95 °C	15 sec	16
60 °C	4 min	cycles
99.9 °C	10 min	
4 °C	~	

2.7. MiRNA expression profiling by Array Cards

Custom TaqMan microRNA Array Cards (ThermoFisher Scientific), quantitative real-time PCR-based cards were used for miRNA expression profiling. They contain assays for the detection of 44 human miRNAs of interest, 2 endogenous reference miRNAs (RNU6, miR-484) and 1 exogenous reference miRNA (cel-miR-39-3p) for data normalization, as well as a N/A-4343438-Blank (negative control). Forty four miRNAs which have been described to be clinically relevant for EOC in the literature and in our previous studies were selected (16, 48). These miRNAs of interest were then mounted on miRNA array cards (ThermoFisher Scientific) and are as followed:

miRBase ID	Target sequence
hsa-let-7g-5p	UGAGGUAGUAGUUUGUACAGUU
hsa-miR-9-5p	UCUUUGGUUAUCUAGCUGUAUGA
hsa-miR-16-5p	UAGCAGCACGUAAAUAUUGGCG
hsa-miR-20a-5p	UAAAGUGCUUAUAGUGCAGGUAG
hsa-miR-21-5p	UAGCUUAUCAGACUGAUGUUGA
hsa-miR-23a-3p	AUCACAUUGCCAGGGAUUUCC
hsa-miR-23b-3p	AUCACAUUGCCAGGGAUUACC
hsa-miR-26a-5p	UUCAAGUAAUCCAGGAUAGGCU
hsa-miR-27a-3p	UUCACAGUGGCUAAGUUCCGC

hsa-miR-27b-3p	UUCACAGUGGCUAAGUUCUGC
hsa-miR-29a-3p	UAGCACCAUCUGAAAUCGGUUA
hsa-miR-30c-5p	UGUAAACAUCCUACACUCUCAGC
hsa-miR-34c-5p	AGGCAGUGUAGUUAGCUGAUUGC
hsa-miR-92a-3p	UAUUGCACUUGUCCCGGCCUGU
hsa-miR-93-5p	CAAAGUGCUGUUCGUGCAGGUAG
hsa-miR-100-5p	AACCCGUAGAUCCGAACUUGUG
hsa-miR-103a-3p	AGCAGCAUUGUACAGGGCUAUGA
hsa-miR-126-3p	UCGUACCGUGAGUAAUAAUGCG
hsa-miR-141-3p	UAACACUGUCUGGUAAAGAUGG
hsa-miR-152	UCAGUGCAUGACAGAACUUGG
hsa-miR-182-5p	UUUGGCAAUGGUAGAACUCACACU
hsa-miR-187-3p	UCGUGUCUUGUGUUGCAGCCGG
hsa-miR-191-5p	CAACGGAAUCCCAAAAGCAGCUG
hsa-miR-200a-3p	UAACACUGUCUGGUAACGAUGU
hsa-miR-200b-3p	UAAUACUGCCUGGUAAUGAUGA
hsa-miR-200c-3p	UAAUACUGCCGGGUAAUGAUGGA
hsa-miR-203	GUGAAAUGUUUAGGACCACUAG
hsa-miR-205-5p	UCCUUCAUUCCACCGGAGUCUG
hsa-miR-214-3p	ACAGCAGGCACAGACAGGCAGU
hsa-miR-221-3p	AGCUACAUUGUCUGCUGGGUUUC
hsa-miR-223-3p	UGUCAGUUUGUCAAAUACCCCA
hsa-miR-320a	AAAAGCUGGGUUGAGAGGGCGA
hsa-miR-373-3p	GAAGUGCUUCGAUUUUGGGGUGU
hsa-miR-422a	ACUGGACUUAGGGUCAGAAGGC
hsa-miR-429	UAAUACUGUCUGGUAAAACCGU
hsa-miR-485-5p	AGAGGCUGGCCGUGAUGAAUUC
hsa-miR-496	UGAGUAUUACAUGGCCAAUCUC
hsa-miR-519a-3p	AAAGUGCAUCCUUUUAGAGUGU
hsa-miR-520g	ACAAAGUGCUUCCCUUUAGAGUGU
hsa-miR-548a-3p	CAAAACUGGCAAUUACUUUUGC
hsa-miR-574-3p	CACGCUCAUGCACACACCCACA
hsa-miR-590-5p	GAGCUUAUUCAUAAAAGUGCAG
hsa-miR-625-5p	AGGGGGAAAGUUCUAUAGUCC
hsa-miR-891a	UGCAACGAACCUGAGCCACUGA

To carry out real-time TaqMan PCR, the protocol of Thermo Fisher Scientific was modified as followed: The 112.5-µl PCR reaction containing 56.25 µl TaqMan Universal Master Mix II and 2 µl preamplication product was loaded on the array cards. PCR was run on a 7900 HT Fast Real-Time PCR System (Applied Biosystems): 1 cycle at 95 °C for 10 min; 40 cycles at 95 °C for 15 s, and 60 °C for 1 min.
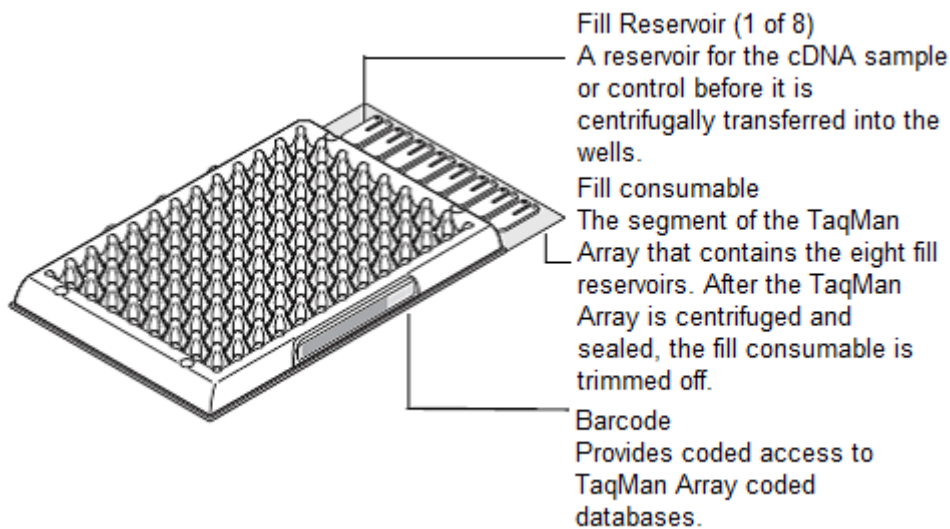
Figure 2.2. TaqMan microRNA Array Cards (Applied Biosystems)

Samples are loaded onto cards and centrifugally transferred into the wells. The cards are sealed by a sealer (Applied Biosystems). Then, the cards are trimmed off, and run on a 7900 HT Fast Real-Time PCR System.

2.8. Transient transfection of cell lines

MiRNA mimics are chemically synthesized miRNAs, and can function as mature miRNAs after transfection into the cell. They can bind to the 3'-UTR of their target mRNAs and mediate mRNA destruction. MiRNA inhibitors are single-stranded, modified RNAs, they specifically inhibit miRNA function after transfection. Transfection of miRNA mimics or inhibitors is used to identify their mRNA targets and investigate their functions.

For the transient transfection, 1.5×10^5 SKOV3 or 1.0×10^5 OVCAR8 cells were seeded per well on 6-well plates (for cell proliferation assays) and 4,000 SKOV3 or 8,000 OVCAR3 cells were seeded in triplicate per well into a 96-well plate (for apoptosis assays) one day before

transfection. The next day, these cell lines were transfected with double-stranded miScript miRNA mimic (Qiagen, Hilden, Germany), single-stranded miScript inhibitor (Qiagen) (miR-200b or miR-320) or AllStars negative control small interfering RNA (negative control) (Qiagen) at final concentrations of 10, 50 or 10 nM, respectively, together with 4.5 µl (for apoptosis assays) or 0.75 µl (for cell proliferation assays) HiPerFect® Transfection Reagent (Qiagen).

2.9. Western Blotting: Protein quantification

To calculate the adequate protein amounts for carrying out a Western blot, the protein concentrations were at first measured with the DC Protein Assay Kit (BioRad, Munich, Germany) at a wavelength of 650 nm on a spectrophotometric plate reader (Tecan). A standard curve of 0, 0.625, 1.25, 2.5, 5 and 10 mg/ml BSA (bovine serum albumin; Sigma Aldrich Chemie, Munich, Germany) was applied by the double-dilution method. Three µl of exosomes, exosome supernatant and BSA standard protein samples were added to 96-well plates, and incubated with a mixture of 25 µl Reagent A, 0.5 µl Reagent S and 200 µl Reagent B. After 15-min incubation at room temperature (RT), the plate was measured at a wavelength of 650 nm on a microplate reader. The obtained OD optical density values and the corresponding concentrations of BSA standard protein samples generated a linear equation of $y = mx + n$, as calculated by a linear regression analysis. The R^2 near to 1 was also calculated to indicate the fitness of the linear equation. The concentrations of target protein samples were calculated according to this equation of standard.

2.10. Western Blotting: SDS polyacrylamide gel electrophoresis

Sodium dodecyl sulfate polyacrylamide gel electrophoresis (SDS-PAGE) is a technique used for separation of proteins based on their molecular weights (measured in kilo Daltons, kDa). SDS binds to and denatures proteins, and charges them negatively. When gel electrophoresis starts, all proteins migrate through the gel towards the anode core. Proteins with lower molecular weight migrate quicker than those with higher molecular weight. The gel consists of a resolving and a stacking gel. The stacking gel allows proteins to be

concentrated into a tight band at the beginning of electrophoresis, and to be separated from the starting line before they migrate through the resolving gel. The components of the 10 % resolving gel and stacking gel are as followed:

Component	10 % resolving gel	stacking gel
Double-distilled water	5.9 ml	2.7 ml
30 % Polyacrylamide	5.0 ml	670 µl
1 M Tris (pH 6.8)		500 µl
1.5 M Tris (pH 8.8)	3.8 ml	
10 % SDS	150 µl	40 µl
Tetramethylethylenediamine	6.0 µl	5.0 µl
10 % ammonium persulfate	150 µl	40 µl

About 30 µg proteins mixed with 6 x Loading Buffer (Carl Roth GmbH + Co. KG, Karlsruhe, Germany) were used for Western blotting. The maximum volume of the mixture should not exceed 25 µl because of the limited size of gel slots. The protein mixture was denatured at 95 °C for 10 min. An XCell SureLock® Mini-Cell device (Life Technologies) and 1 x Laemmli Running Buffer were used for gel electrophoresis. Seven µl PageRuler™ Plus Prestained Protein Ladder (Thermo Scientific) was used to determine the different molecular weights of the separated proteins. The running time depends on the molecular weight of a protein. Normally, it takes 1-2 h at 100 V.

2.11. Western Blotting: PVDF membrane transferring

After gel electrophoresis, the separated proteins in the gel were transferred onto a PVDF (polyvinylidene fluoride) membrane (0.45 µm) on an XCell II™ Blot Module (Life Technologies). First, the PVDF membrane was activated with methanol for 1 min, then incubated with double-distilled water for 3 min and soaked in transfer buffer for 5 min. Blotting pads and filter papers were presoaked with transfer buffer before placing in the cathode core of the XCell II™ Blot Module. In the module, two blotting pads, filter paper, gel, PVDF membrane, filter paper and two blotting pads were stacked from the cathode core to the anode core (Figure 2.3.). The air bubbles between the pads, especially between the gel

and PVDF membrane, were removed by a glass rod before placing the gel membrane sandwich and blotting pads in the cathode core of the XCell II™ Blot Module. The assembled chamber was filled with transfer buffer, and the outside of the chamber was surrounded with cold tap water. It normally takes 1 h to finish the transfer at 25 V. The components of 1 x Laemmli Running Buffer and transfer buffer are as followed:

Components	1 x Laemmli Running Buffer	transfer buffer
Tris	3.02 g	5.81 g
20 % SDS	5 ml	1.85 ml
Glycine	14.42 g	2.93 g
20 % Methanol		200 ml
ddH$_2$O	1000 ml	1000 ml
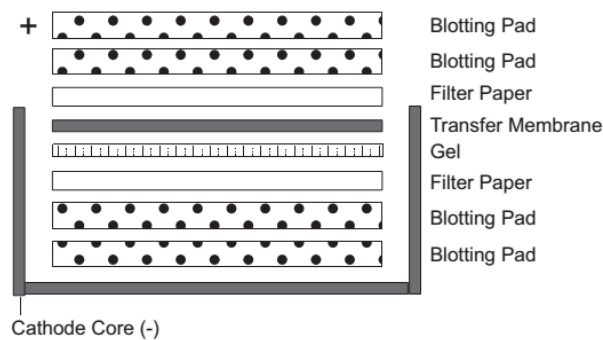
Figure 2.3. Schematic structure of the XCell II™ Blot Module (from "Western Blotting Using PVDF Membranes protocol" of Invitrogen)

The proteins are transferred from the gel (cathode) to the PVDF membrane (anode).

2.12. Western Blotting: Immunodetection

The PVDF membrane with the transferred proteins was first blocked with 6 % milk solution (6 g milk powder in 100 ml TBST buffer) or 5 % BSA solution (5 g BSA in 100 ml TBST buffer), in a 50 ml-tube, at RT for 1 h, to avoid non-specific antibody binding resulting in non-specific signals on the exposed film. Then, the PVDF membrane was incubated overnight at 4 °C with the first antibody diluted in 5 ml 6 % milk solution or 5 % BSA solution. Dilutions of the first antibodies are as followed:

First antibodies	Molecular weight	Dilutions
CD63 (ABGENT)	35-55 kDa	1:1 000 (in 6 % milk)
AGO2 (TAKARA)	103 kDa	1:2 000 (in 5 % BSA)

On the next day, the PVDF membrane was washed for 3 x 10 min with TBST buffer, and subsequently incubated with a secondary antibody at RT for 1 h. The used secondary antibodies are as followed:

Secondary antibodies	Dilutions
Anti-rabbit immunoglobulins HRP (Dako)	1:2 000 (in 6 % milk)
Anti-mouse immunoglobulins HRP (Dako)	1:2 000 (in 5 % BSA)

The secondary antibody binds to the primary antibody which is specifically bound to the protein of interest. Since the secondary antibody is linked to horseradish peroxidase (HRP), which cleaves a chemiluminescent agent, the reaction product produces luminescence (Figure 2.4.). The light is trapped by a photosensitive X-ray film (GE Healthcare) (49). After incubation with the secondary antibody, the PVDF membrane was washed with TBST buffer for 3 x 10 min, again. Then the PVDF membrane was incubated at RT for 4 min with the mixture of reagent I and reagent II. The chemiluminescent signals were detected on a photosensitive X-ray film (GE Healthcare). The exposure time varied from 30 sec to 5 min. It depended on the signal strength of the protein. The films were developed in an X-ray film developer Curix60, and scanned on an EPSON perfection V750 PRO device. The chemiluminescent agent was prepared as followed:

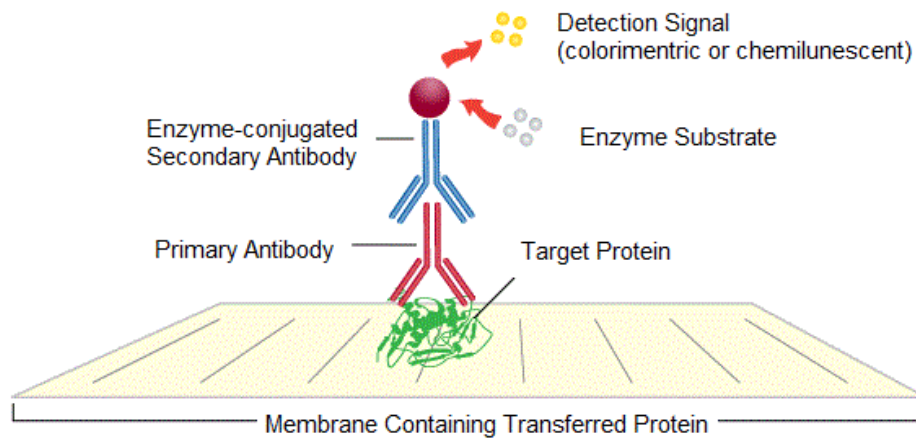| Reagent I		Reagent II	
Luminol	100 µl	Tris/HCl pH8.5	1 ml
p-Coumaric	44 µl	30 % H_2O_2	6 µl
Tris/HCl pH8.5	1 ml	Water	9 ml
Water	8.85 ml		

Figure 2.4. Detection of specific protein by Western Blot (modified from General Western Blot Protocol, Leinco Technologies, Inc.)

The target protein is bound to the primary antibody. Enzyme-conjugated secondary antibody binds to the primary antibody. Then, the protein-antibodies-enzyme complex cleaves a chemiluminescent agent and produces luminescence which can be detected by a photosensitive X-ray film (GE Healthcare).

2.13. Proliferation MTT assay

The MTT assay is used for assessing cell metabolic activity. The number of viable cells is referred to the cellular NAD(P)H-dependent oxidoreductase enzymes. These enzymes are capable of reducing the tetrazolium dye MTT (3-(4,5-dimethylthiazol-2-yl)-2,5-diphenyltetrazolium bromide) to the insoluble purple formazan. The insoluble purple formazan can be solubilized by lysis buffers [e.g., DMSO (dimethylsulfoxide) or NP-40 (tergitol-type NP-40, nonyl phenoxypolyethoxylethanol)]. The spectrophotometer is applied to measure the concentration of the solubilized cells at OD 540 nm together with a reference at 650 nm. Thus, to investigate the influence of miRNAs on the proliferation of EOC cell lines, I performed this assay. Two hundred µl of SKOV3 and OVCAR3 cells were seeded at densities of 4,000 and 8,000 cells per well into 96-well plates, respectively. After 24 h the cell lines were transiently transfected with double-stranded miScript miRNA mimics or single-stranded miScript inhibitors miR-200b and miR-320 or AllStars negative control small interfering RNA (negative control) at final concentrations of 10, 50 or 10 nM, respectively,

with 0.75µl HiPerFect® Transfection Reagent (Qiagen, Hilden, Germany). After 24 h, 48 h and 72 h incubation, 20 µl MTT solution was added to each well, and incubated at 37°C for 3 h. Then, the media were discarded completely, and cells were solubilized with 150 µl lysis buffer (4 mM HCl, 0.1% NP-40 in isopropanol). After dissolving the cells, the microplate reader Sunrise was used to measure the OD value of each well at 540 nm, together with a reference at 650 nm.

2.14. Apoptosis assay by FACS

Apoptosis is a normal physiologic process of programmed cell death which occurs in multicellular organisms. This process leads to characteristic cell changes including loss of plasma membrane, condensation of the cytoplasm and nucleus, chromosomal DNA fragmentation, global mRNA decay and final cell death. In the early stage of apoptotic cells, the membrane phospholipid phosphatidylserine (PS) is translocated from the inner to the outer leaflet of the plasma membrane, thereby exposing PS to the external cellular environment. Annexin V, a 35-36 kDa Ca^{2+} dependent phospholipid–binding protein, has a high affinity for PS, and bind to the exposed PS. Since Annexin V is conjugated to fluorochromes, such as FITC, it can be measured by flow cytometry. Based on the externalization of PS in the early stages of apoptosis, FITC Annexin V staining can identify apoptosis at early stages. Viable cells with intact membranes exclude propidium iodide (PI), a DNA dye, whereas the membranes of dead and damaged cells are permeable to PI. Therefore, the assay can identify not only early but also late apoptotic cells. For example, early apoptotic cells are FITC Annexin V positive and PI negative, and late apoptotic cells are FITC Annexin V positive and PI positive (Figure 2.5). The influence of a particular miRNA on apoptosis was examined by this assay along with FACS (fluorescence-activated cell sorting).
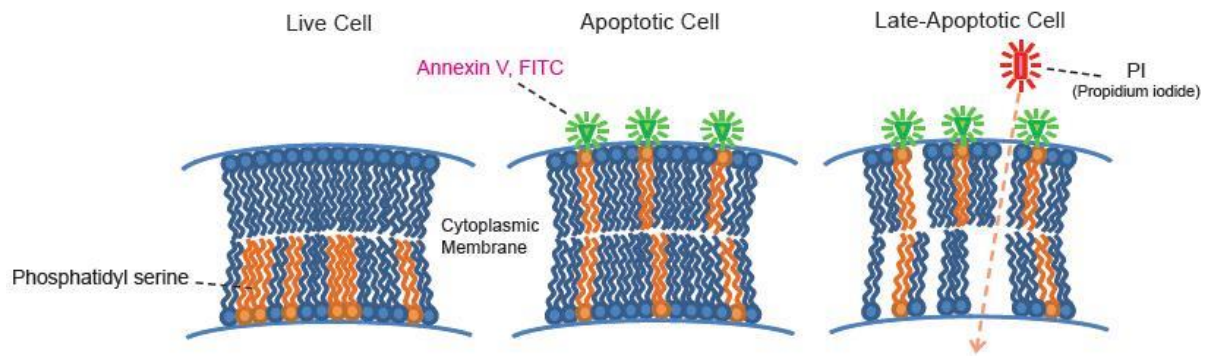
Figure 2.5. Apoptosis of cells (from Annexin V, FITC apoptosis detection kit, Dojindo, EU GmbH)

The cell membrane is shown with the early and late apoptotic markers.

In my experiment, I used camptothecin to induce apoptosis. Camptothecin is a topoisomerase I inhibitor, it binds to the covalent complex of topoisomerase I and DNA resulting in a stable ternary complex. The inhibition of DNA re-ligation causes DNA damage which leads to apoptosis. Two ml of 1.5×10^5 SKOV3 or 1.0×10^5 OVCAR8 cells were seeded into each well of 6-well plates. Next day, cells were transfected with double-stranded miScript miRNA mimics, single-stranded miScript inhibitors (miR-200b or miR-320) or AllStars negative control small interfering RNA (negative control) at final concentrations of 10, 50 or 10 nM, respectively, with 4.5 µl HiPerFect® Transfection Reagent (Qiagen, Hilden, Germany). After 24-h incubation, 10 µl 5 mM camptothecin (BioVision) were added to SKOV3 and OVCAR3 cells per well to induce apoptosis. After 4-h apoptosis induction, camptothecin was removed by normal medium. Cells were harvested using trypsin and washed with 2 x PBS (Life Technologies) on the 4th day. Centrifuged cell pellets were resuspended in 100 µl 1 x binding buffer (Annexin V FITC Apoptosis Detection Kit, BD Biosciences), and stained with 5 µl Annexin V and 5 µl PI (Annexin V FITC Apoptosis Detection Kit, BD Biosciences) for 15 min at RT. Staining was performed in the dark. In addition, a tube containing unstained cells solved in binding buffer was used to adjust the FACS Canto II device and system. In the FACS Canto II device (BD Biosciences), the cells were stimulated by a laser at a wavelength of 488 nm. Annexin V- FITC stained cells were detected by a 585/42 filter (long pass mirror of 556 nm), while PI stained cells were detected

by a 660/20 filter (long pass mirror of 610 nm). The data were analyzed using the FACS Diva software.

2.15. Data normalization and statistical analyses

The statistical analyses were performed using the Thermo Fisher Scientific Analysis Software, Relative Quantification Analysis Module, version 3.1 (www.aps.thermofisher.com), and SPSS software package, version 22.0 (SPSS Inc. Chicago, IL). First, the obtained data of the miRNA expression levels were calculated and evaluated by the ΔCq method as follows: ΔCq = mean value Cq (reference miR-484) - mean value Cq (miRNA of interest). For data normalization, snRNU6 could not be used as a reference because its expression was too instable, whereas the expression of miR-484 remained relatively constant across the plasma samples. The interindividual variability controlled by spiking in of cel-miR-39-3p was low.

The Thermo Fisher Scientific Analysis Software was used for performing hierarchical clustering (heat map) and volcano plots. Distances between samples and assays were calculated for hierarchical clustering based on the ΔCq values using Pearson's Correlation. Clustering method was average linkage. Subsequently, the relative expression data were 2^ΔCq transformed in order to obtain normal distribution data. The confidence of 2^ΔCq data were verified by amplification curves and Cq confidence (0-1), whereby 1 refers to the highest confidence. My data showed a Cq confidence of 0.95. Values below 0.95 were discarded.

Statistical difference of miRNA expressions between healthy controls, ovarian cystadenoma patients and EOC patients were calculated using two-tailed student t-test and depicted as a volcano plot. Diagnostic power of the exosomal miRNAs was analyzed by receiver operating characteristic (ROC) curves. The correlations of plasma levels of exosomal miRNAs with clinical parameters were detected by using ANOVA Tukey's HSD test and Spearman-Rho test. Univariate and multivariate analyses were performed for prognostic factors of overall survival using the Cox regression model. To estimate overall and disease-free survival, Log rank test and Kaplan-Meier plots were carried out. The impacts of miRNAs on cell

proliferation and apoptosis were analyzed by using ANOVA Tukey's HSD test, and line charts and bar charts were drawn. Missing data were handled by pairwise deletion. A p-value <0.05 was considered as statistically significant.

3. Results

3.1. Workflow

First, I used real-time PCR-based miRNA array cards to quantify 44 miRNAs (plus 4 references) in exosomes derived from plasma samples of 106 EOC patients, 8 ovarian cystadenoma patients and 29 healthy women. The clinical parameters of plasma samples are described in Table 3.1. Exosomes were verified by a Western blot. Following the quantification of exosomal miRNAs, the array data were normalized by an endogenous reference miRNA-484, because this reference miRNA displayed constant values through the cohorts of EOC patients, ovarian cystadenoma patients and healthy women. The interindividual variability was controlled by spiking in cel-miR-39-3p. The normalized data were statistically evaluated and compared with the clinical parameters of the EOC patients. Then, the impact of miR-200b and miR-320 on cell proliferation and apoptosis were analyzed in cell culture experiments. I selected these miRNAs because they were significantly deregulated in exosomes from EOC patients, and their dual character as tumor suppressor genes and oncomiRs with multiple cancer-specific functions have been described in diverse studies. Figure 3.1 summarized the single steps of the workflow.
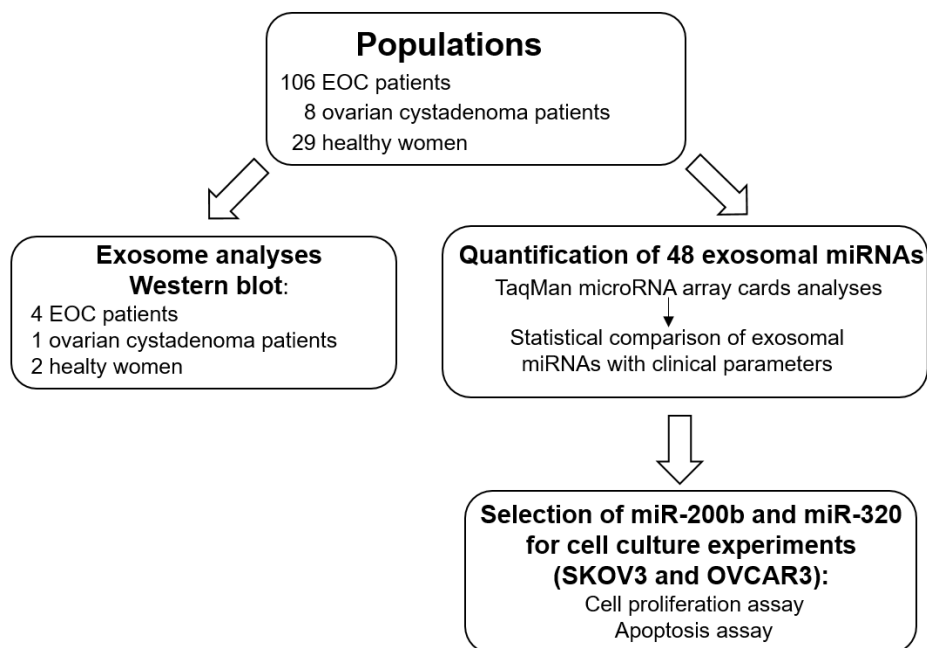
Figure 3.1. Workflow of the study

Table 3.1. Clinical characteristics of EOC patients and ovarian cystadenoma patients and healthy women

Ovarian cancer patients	106(100%)
Age (mean)	60 (28-81 years)
Follow-up time (median)	22 (0-247 months)
Recurrence	
Yes	49(46.2%)
No	57(53.8%)
Histology	
Serous	90(84.9%)
Other subtypes	13(12.3%)
unkonwn	3 (2.8%)
FIGO-stage	
I-III	72(67.9%)
IV	20(18.9%)
unkonwn	14(13.2%)
Grading	
G1-2	25(23.6%)
G3	72(67.9%)
unkonwn	9 (8.5%)
Lymph node	
N0	17(16.1%)
N1	56(52.8%)
unkonwn	33(31.1%)
Secondary carcinoma	
Yes	18(17.0%)
No	88(83.0%)
Tumour residual	
Tumor-free	61(57.5%)
Tumor rest	38(35.8%)
unkonwn	7 (6.6%)
Disease-freeurvival(months)	16.6(0-84)
CA 125 U/ml	
<65	5 (4.7%)
≥65	69(65.1%)
unknown	32(30.2%)
Survival status	
Dead	35(33.0%)
Alive	71(67.0%)
Benign patients	8
Age (mean)	61(45-81 years)
Healthy women	29
Age (mean)	56(47-69 years)

3.2. Verification of exosomes

Before I quantified exosomal miRNAs, the extracted exosomes from 2 healthy women, 1 ovarian cystadenoma patient and in each case 2 EOC patients at FIGO stage III and IV were verified on a Western Blot using antibodies specific for the exosomal marker CD63 and the miRNA binding protein AGO2. As shown by the 45 kDa-band on the blot, the CD63-specific antibody recognized non-lysed exosomes in the pellet. Strikingly, the exosome bands were stronger in the cystadenoma patient and EOC patients at FIGO stage IV than in healthy women and EOC patients at FIGO stage III (Figure 3.2A). As shown by the 103 kDa-band on the blot, the AGO2-specific antibody did not detect AGO2 protein which is bound to cell-free miRNAs in the exosome pellet (Figure 3.2B). These findings show that the exosome fraction may be pure and devoid of cell-free miRNAs. However, they do not exclude that exosomes may contain traces of contaminations of cell-free AGO2-bound miRNAs and that due to the low sensitivity of the Western blot were not detectable.

Figure 3.2. Verification and quantification of exosomes
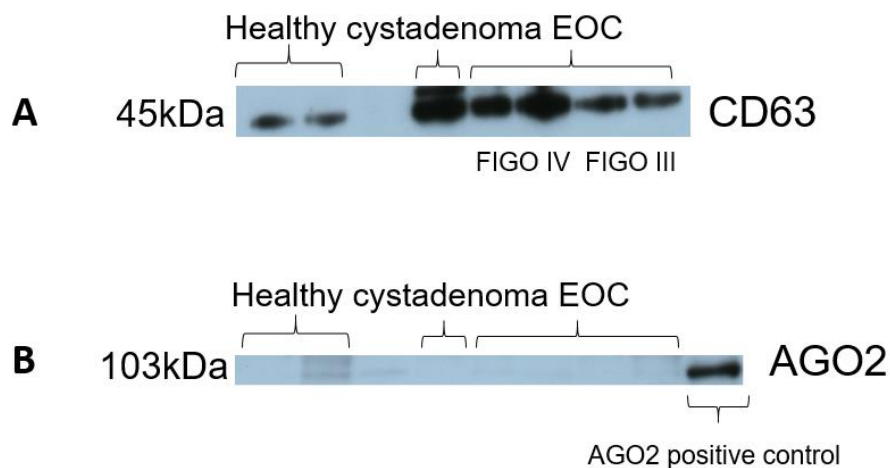
Exosomes were precipitated from plasma of healthy women, ovarian cystadenoma patients and EOC patients by the agglutinating agent ExoQuick and analyzed by Western blots using antibodies specific for the exosome proteins CD63 (**A**), and the miRNA-associated AGO2 protein (**B**). The Western blots show representative examples of exosomes, devoid of cell-free miRNAs.

3.3. Different miRNA signatures in exosomes of EOC patients and ovarian cystadenoma patients

Next, I used a quantitative TaqMan real-time PCR-based cards containing 48 different miRNAs, to determine the miRNA expression profiles in exosomes derived from the plasma of 106 EOC patients, 8 ovarian cystadenoma patients and 29 healthy women. The selected miRNAs are listed in Materials and Methods. Then, a similarity matrix was generated containing all pairwise similarities of the plasma samples of EOC patients, ovarian cystadenoma patients and healthy controls. Hierarchical clustering was carried out to detect potential clusters in rows (miRNAs) and columns (plasma samples) of the normalized expression matrix. The relative up- and downregulated miRNAs are indicated by red and green, respectively (heat map, Figure 3.3).

Figure 1.3.4 shows the volcano plots, I compared the enrichment of miRNAs in exosomes derived from plasma of 106 EOC with that of 29 healthy women (Figure 3.4A), 106 EOC with that of 8 ovarian cystadenoma patients (Figure 3.4B) and 8 ovarian cystadenoma patients with that of 29 healthy women (Figure 3.4C). And table 1.3.2 summarizes the significant results with the adjusted p-values and fold changes of miRNAs as derived from the heat map (Figure 3.3) and volcano plots (Figure 3.4). According to the results, from 44 miRNAs, 4 miRNAs (miR-21, miR-100, miR-200b and miR-320) were significantly enriched, whereas 4 miRNAs (miR-16, miR-93, miR-126 and miR-223) were under-presented in exosomes of EOC patients compared with those of healthy women. The levels of exosomal miR-23a and miR-92a were significantly lower in plasma of ovarian cystadenoma patients than in healthy women and EOC patients (Figure 3.4, Table 3.2).

In addition, I carried out ROC analyses of the most deregulated miRNAs. The significant differences of exosomal miRNA concentrations between EOC patients and healthy women were reflected by the AUC values of miR-21 (0.740), miR-200b (0.868), and miR-320 (0.658). I also calculated the sensitivity and specificity of these exosomal miRNAs by the highest Youden index. The levels of exosomal miR-21 and miR-200b could best discriminate between EOC patients and healthy women with a sensitivity of 61% and 64% and a

specificity of 82% and 86% (Figure 3.5A & B). However, the levels of exosomal miR-320 (0.658) only showed a sensitivity of 56% and a specificity of 69% between EOC patients and healthy women. The combination of the concentrations of exosomal miR-21 and miR-200b could not increase the sensitivity and specificity (data not shown).
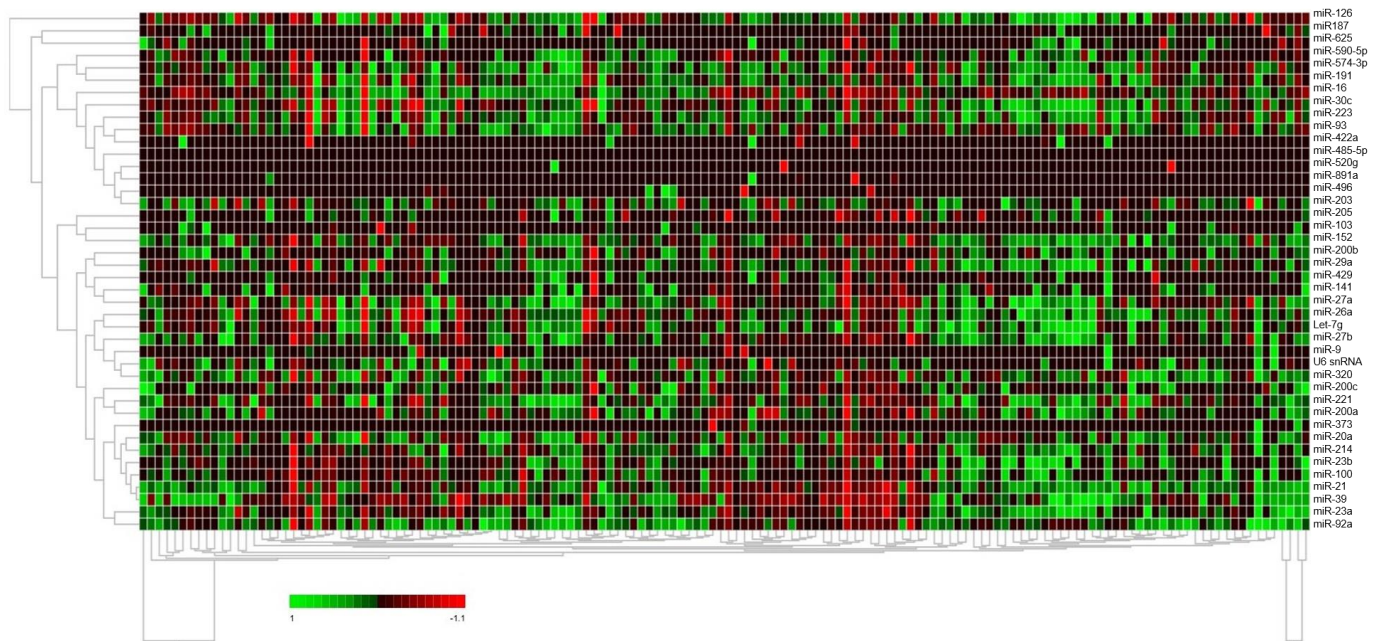
Figure 3.3. Hierarchical cluster of 48 exosomal miRNAs

The heat map is derived from data of the miRNA arrays which were performed using quantitative real-time PCR based array cards mounted with assays for detection of 48 different miRNAs and using exosome samples from plasma of 106 EOC patients, 8 ovarian cystadenoma patients and 29 healthy women. The colored representation of samples and probes is ordered by their similarity. The red and green colors indicate that the ΔCq value is below (relatively high expression) and above (relatively low expression levels) the median of all ΔCq values in the study, respectively. On top: clustering of samples. On the right side: clustering of probes. The scale bar provides information on the degree of regulation.
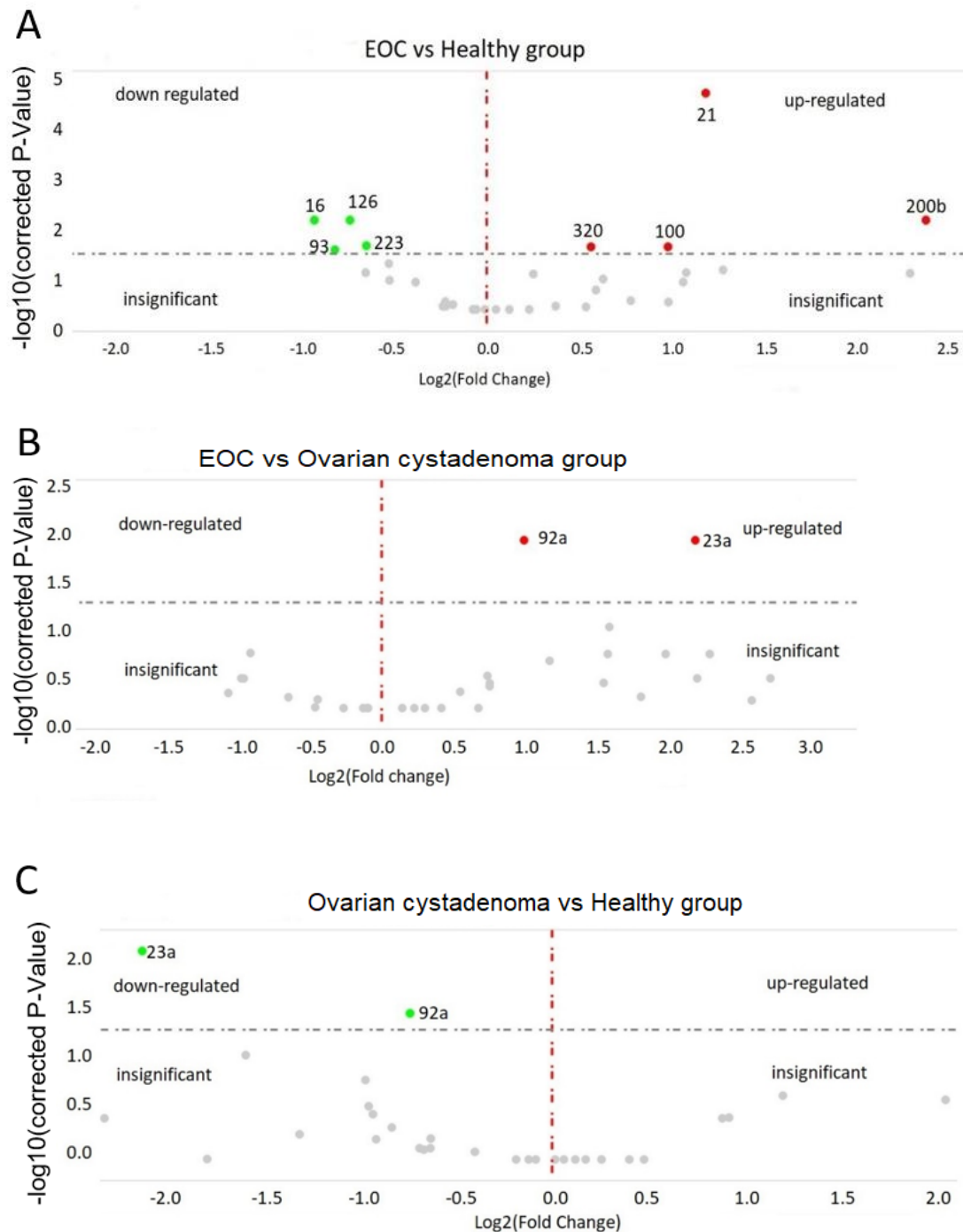
Figure 3.4. Volcano plots of exosomal miRNAs

The plots were drawn for comparison of exosomal miRNAs in plasma of 106 EOC patients with those of 29 healthy women (**A**) and 8 ovarian cystadenoma patients (**B**) as well as between ovarian cystadenoma patients and healthy women (**C**). The Log2 fold changes are plotted on the x-axis and the negative log10 p-values are plotted on the y-axis. The left side shows downregulated exosomal miRNAs (green dots). The right side shows upregulated

exosomal miRNAs (red dots). Under the dashed horizontal line there are non-deregulated miRNAs (grey dots).

Table 3.2. Summary of the significant results with the adjusted p-values and fold changes of miRNAs as derived from the heat map (Figure 3.3) and volcano plots (Figure 3.4), and the comparision of clinical parameters with the expression of exosomal miRNAs in EOC patients

populations	Patients No.		miR-16	miR-21	miR-23a	miR-92a	miR-93	miR-100	miR-126	miR-200b	miR-200c	miR-223	miR-320
EOC vs healthy	106 vs 29	fold change	**0.5**	**2.3**	1.0	1.2	**0.5**	**2.0**	**0.6**	**5.2**	4.9	**0.6**	**1.5**
		p-value	**0.009**	**0.0001**	1.000	0.148	**0.014**	**0.034**	**0.012**	**0.008**	0.143	**0.029**	**0.034**
EOC vs cystadenoma	106 vs 8	fold change	0.9	3.0	**4.6**	**2.0**	0.9	12.4	0.5	2.3	3.5	0.7	1.5
		p-value	1.0	0.100	**0.009**	**0.009**	1.000	0.210	0.210	0.261	0.725	0.976	0.630
cystadenoma vs healthy	8 vs 29	fold change	0.6	0.8	**0.2**	**0.6**	0.6	0.2	1.1	2.3	1.4	0.9	1.0
		p-value	0.478	0.839	**0.008**	**0.034**	0.770	0.177	1.000	0.229	1.000	1.000	1.000
Clinical parameters in EOC patients													
Recurrence	Yes 48	fold change	**0.5**	1.1	1.0	0.8	0.6	1.4	1.0	1.3	1.1	0.8	0.9
	No 54	p-value	**0.001**	0.648	0.845	0.073	0.05	0.224	0.780	0.710	0.841	0.366	0.717
Histology	serous 90	fold change	0.7	**0.5**	0.7	**0.7**	0.7	0.6	0.7	0.7	0.6	0.7	0.7
	Others 13	p-value	0.432	**0.026**	0.285	**0.010**	0.413	0.192	0.162	0.686	0.289	0.177	0.190
Grading	G1-2 24	fold change	**0.5**	0.8	1.0	0.8	0.7	1.3	1.0	4.1	0.8	1.2	0.8
	G3 69	p-value	**0.019**	0.504	0.995	0.150	0.200	0.341	0.946	0.144	0.524	0.366	0.226
CA125		p-value	0.325	0.377	0.637	0.124	0.415	0.156	0.762	**0.002**	**0.003**	0.835	0.363

A
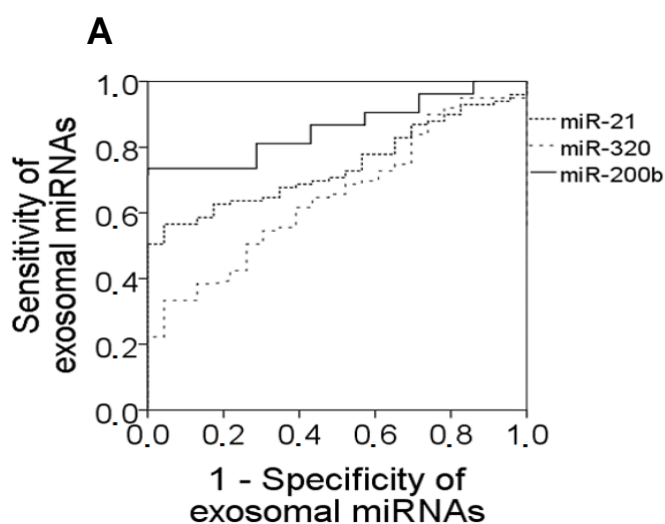
B

miRNAs	AUC	P value	Sensitivity %	Specificity %
miR-21	0.740	0.0001	61%	82%
miR-320	0.658	0.009	56%	69%
miR-200b	0.868	0.001	64%	86%

Figure 3.5. Exosomal miRNAs differ between EOC patients and healthy women

ROC analyses show the profiles of sensitivity and specificity of exosomal miR-21, miR-320 and miR-200b to distinguish EOC patients from healthy women (**A**). The table summarizes sensitivities and specificities of exosomal miR-21, miR-320 and miR-200b (**B**).

3.4. Diagnostic and prognostic relevance of exosomal miRNAs

Table 3.2 also shows the significant correlations of the levels of exosomal miR-16, miR-21 and miR-92a with the clinicopathological/risk parameters of EOC patients. Lower levels of exosomal miR-16 were significantly associated with recurrence (p=0.001) and grading G1-2 (p=0.019). The concentrations of miR-21 (p=0.026) and miR-92a (p=0.010) were lower in exosomes in patients with serious EOC than patients with other histological subtypes (Table 3.2). Moreover, the plasma levels of exosomal miR-200b were also significantly associated with increasing values of the tumor marker CA125 (p=0.002, Figure 3.6A). In addition, the plasma levels of exosomal miR-200c were also significantly associated with the tumor marker CA125 (p=0.003, Table 3.2) albeit they did not significantly differ between EOC patients and healthy women.

To assess the prognostic potential of the plasma levels of exosomal miRNAs in EOC patients, Kaplan-Meier and log-rank models were carried out. The median follow-up time was 22 months (range from 1 to 247 months). For these analyses, EOC patients were grouped in patients with expression levels of exosomal miRNAs which were higher and lower than the median miRNA values. The higher concentrations of exosomal miR-200b above the median miRNA value of 0.0016 were associated with poor overall survival (p=0.019, Figure 3.6B). Besides, a positive nodal status correlated with poor overall survival (p=0.017, Table 3.3).

Table 3.3. Univariate and multivariate analyses for overall survival of EOC patients

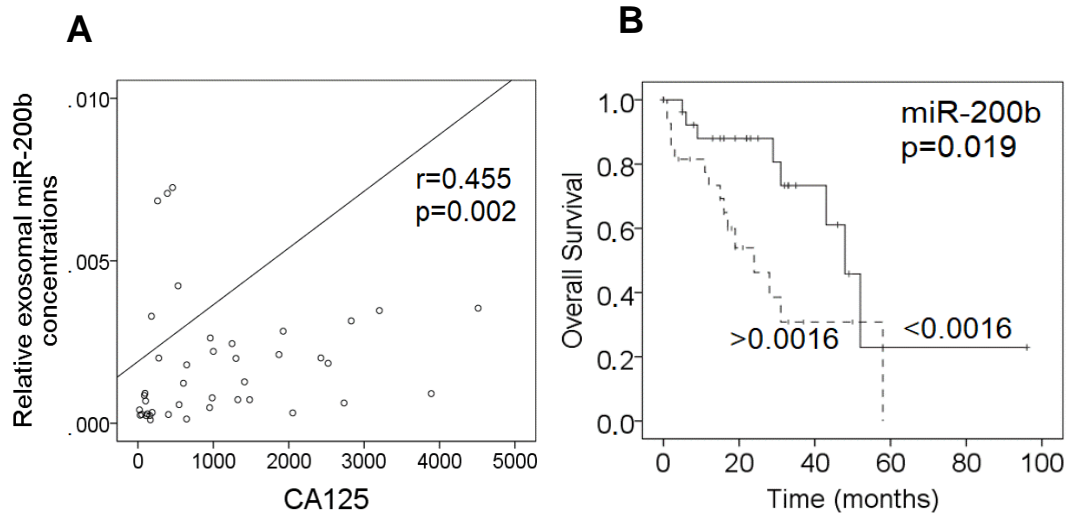| Overall survival	Univariate analysis		Multivariate analysis	
	HR(95% CI) p-values		HR(95% CI) p-values	
Node status(N0,N1)	7.9(1.1-59.1)	**0.017**	-	-
miR-200b	2.7(1.1-6.5)	**0.019**	1.3(0.4-4.2)	0.631

Figure 3.6. **Association of exosomal miR-200b with the tumor marker CA125 and prognosis**

The scatter plot shows the correlation of increasing concentrations of exosomal miR-200b with increasing CA125 values (**A**). The univariate Kaplan-Meier curve shows the correlation of low and high levels of exosomal miR-200b with overall survival. The median value (0.0016) of the exosomal miRNA concentration was used for grouping the EOC samples according to low (n = 28) and high (n = 28) transcript levels (**B**).

3.5. MiR-200b inhibits cell proliferation and promote apoptosis

For cell culture experiments, I selected miR-200b and miR-320. The effects of these miRNAs on cell proliferation and apoptosis were investigated in ovarian cancer cell lines SKOV3 and OVCAR3 which were transiently transfected with mimics and inhibitors of miR-200b and miR-320. Transfection of mimics and inhibitors of miR-200b steadily reduced (p=0.0001) and augmented (p=0.011) cell proliferation in OVCAR3 cells during 72 hours compared with cells transfected with a negative control, indicating that miR-200b inhibits cell proliferation (Figure 3.7A). For the apoptosis assay, the transfected cells were additionally treated with topoisomerase I inhibitor camptothecin. Camptothecin is used in cancer chemotherapy to induce apoptosis. Bright field images and FACS analyses showed that camptothecin and miR-200b mediated apoptosis in OVCAR3 cells (Figure 3.7B&C). The apoptotic effect by camptothecin could still be increased by the additional administration of miR-200b mimics

(p=0.008). However, miR-200b could also induce apoptosis by itself (p=0.021), and this effect was stronger than the effect by camptothecin (p=0.039). Inhibition of miR-200b had no significant impact on cell apoptosis (Figure 3.7B).
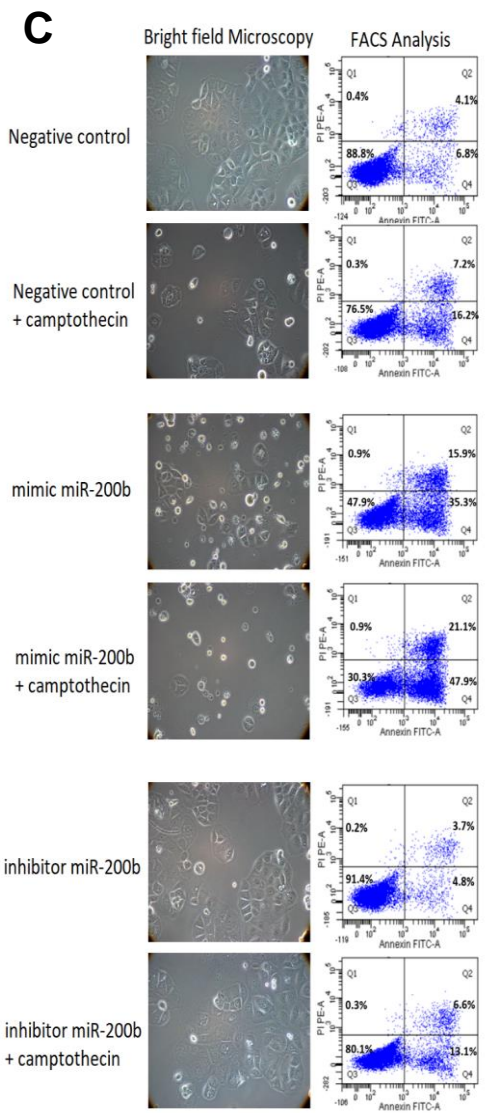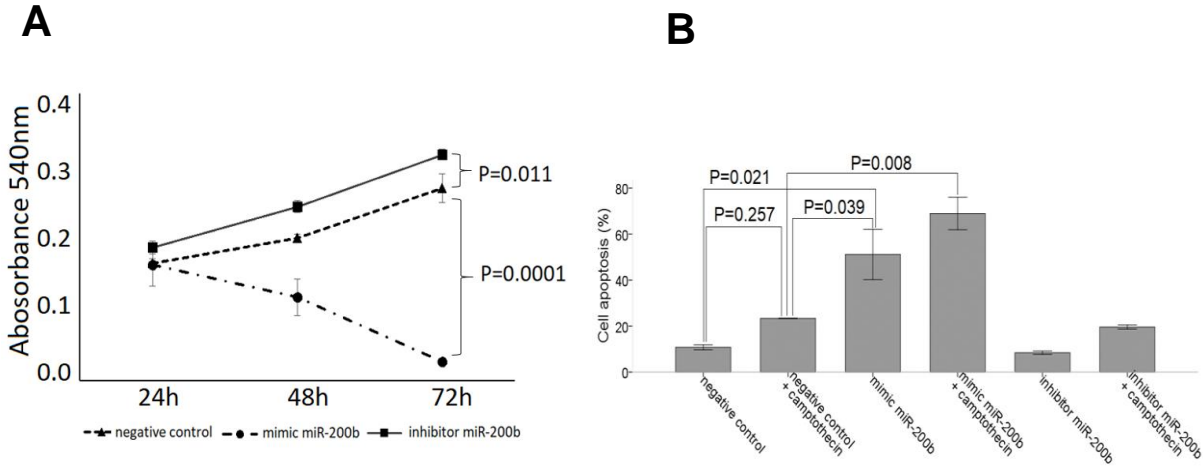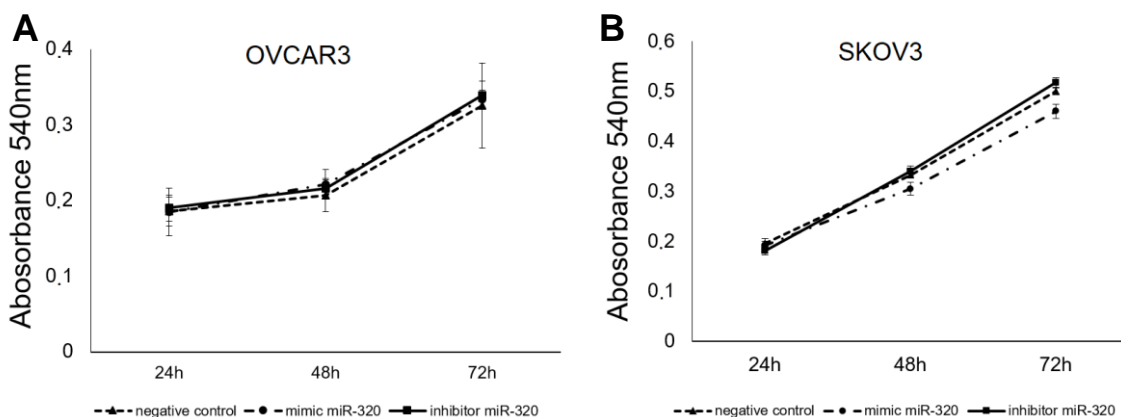
Figure 3.7. MiR-200b affects cell proliferation and apoptosis

OVCAR3 cells were transiently transfected with a negative control, mimic or inhibitor of miR-200b. After 24, 48 and 72 hours, cells were treated with MTT. Cell proliferation after overexpression and inhibition of miR-200b was measured at a absorbance of 540 nm. The standard deviations from triplicate experiments are indicated in the line chart (**A**). Transfected OVCAR3 cells were additionally treated with the topoisomerase I inhibitor camptothecin and analyzed by a bright field microscopy (left) and on a FACS CantoII device (right). In order to observe morphological features of apoptosis cells were analyzed using 10x magnification AxioCam MRc microscope Carl Zeiss. Cells were labeled with Annexin-V-FITC and propidium iodide for FACS analyses. Cell fragments only positive for propidium iodide can be found in the upper left corner (Q1). Late apoptotic as well as necrotic cells can be found in the upper right corner (Q2), since they are positive for Annexin and propidium iodide. Living cells are negative for Annexin and propidium iodide, and therefore, can be found in the lower left corner (Q3). Only early apoptotic cells are positive for Annexin, and located in the lower right corner (Q4). The size for each population (%) is given in the corresponding area (**B**). A bar chart summarizes the data on the apoptotic effect by miR-200b as derived from the FACS CantoII device (**C**).

3.6. MiR-320 has no impact on cell proliferation and apoptosis of OVCAR3 and SKOV3 cells

The other chosen miR-320 had no impact on cell proliferation and apoptosis in both cell lines SKOV3 and OVCAR3 (Figure 3.8).

C **OVCAR3** **D** **SKOV3**

OVCAR3 panel:

negative control
Q1 2.1% Q2 4.5%
Q3 91.1% Q4 2.3%
PI PE-A / Annexin FITC-A

negative control+camptothecin
Q1 3.5% Q2 13.7%
Q3 73.9% Q4 8.9%

mimic miR-320
Q1 5.3% Q2 4.9%
Q3 87.8% Q4 2.1%

mimic miR-320+camptothecin
Q1 4.2% Q2 7.7%
Q3 83.3% Q4 4.9%

inhibitor miR-320
Q1 4.6% Q2 6.4%
Q3 87.5% Q4 1.6%

inhibitor miR-320+camptothecin
Q1 5.9% Q2 7.7%
Q3 82.0% Q4 4.3%

SKOV3 panel:

negative control
Q1 0.0% Q2 1.0%
Q3 96.1% Q4 2.9%

negative control+camptothecin
Q1 0.0% Q2 7.8%
Q3 55.3% Q4 36.9%

mimic miR-320
Q1 0.0% Q2 1.3%
Q3 95.2% Q4 3.5%

mimic miR-320+camptothecin
Q1 0.0% Q2 6.1%
Q3 57.3% Q4 36.6%

inhibitor miR-320
Q1 0.0% Q2 0.8%
Q3 95.7% Q4 3.5%

inhibitor miR-320+camptothecin
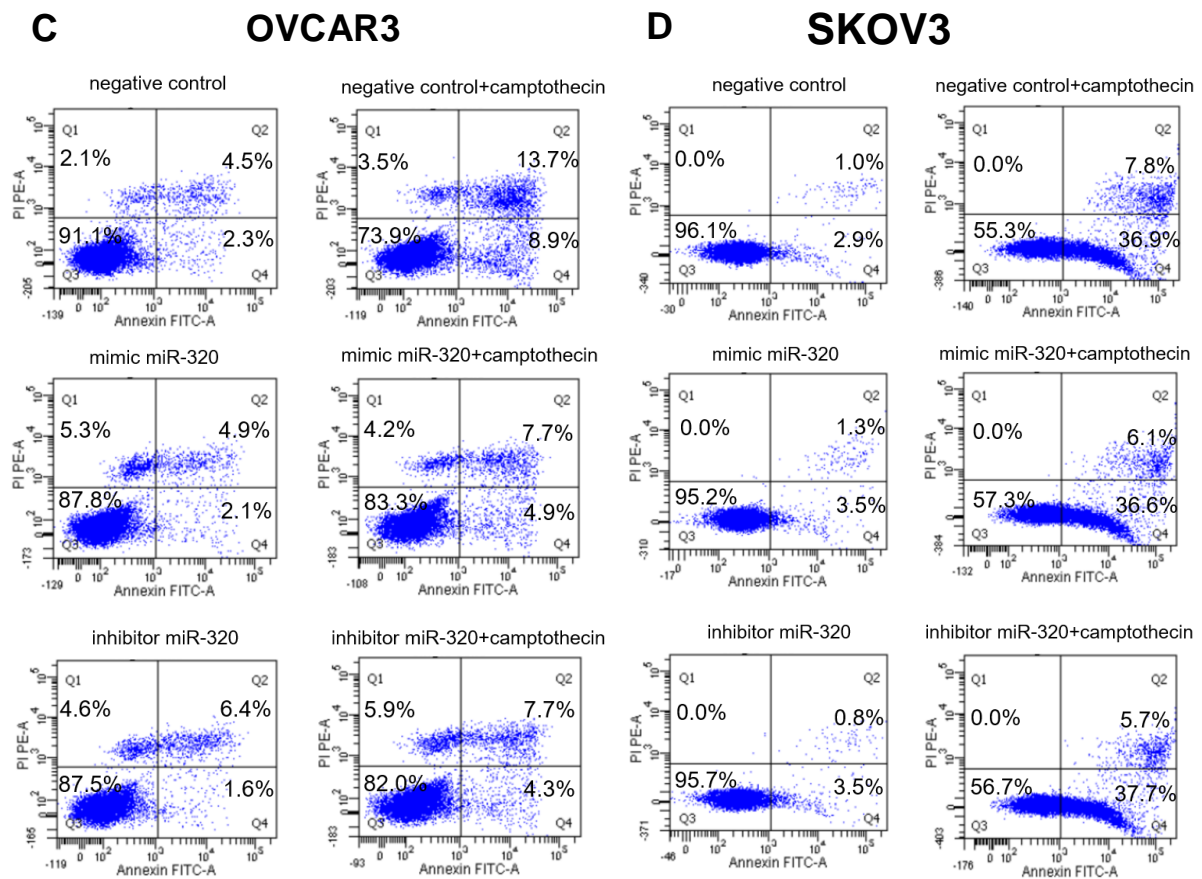Q1 0.0% Q2 5.7%
Q3 56.7% Q4 37.7%

Figure 3.8. MiR-320 has no impact on cell proliferation and apoptosis of SKOV3 and OVCAR3 cells

OVCAR3 and SKOV3 cells were transiently transfected with a negative control, mimic or inhibitor of miR-320. After 24, 48 and 72 hours, cells were treated with MTT. Cell proliferation after overexpression and inhibition of miR-320 was measured at a absorbance of 540 nm. The standard deviations from triplicate experiments are indicated in the line chart (**A** and **B**). Transfected OVCAR3 and SKOV3 cells were additionally treated with the topoisomerase I inhibitor camptothecin and analyzed on a FACS CantoII device for apoptosis. Cells were labeled with Annexin-V-FITC and propidium iodide for FACS analyses. Cell fragments only positive for propidium iodide can be found in the upper left corner (Q1). Late apoptotic as well as necrotic cells can be found in the upper right corner (Q2), since they are positive for Annexin and propidium iodide. Living cells are negative for Annexin and propidium iodide, and therefore, can be found in the lower left corner (Q3). Only early apoptotic cells are positive for Annexin, and located in the lower right corner (Q4). The size for each population (%) is given in the corresponding area (**C** and **D**).

4. Discussion

In the present study, I analyzed the expression of miRNAs in exosomes derived from plasma of EOC and ovarian cystadenoma patients by quantitative TaqMan real-time PCR-based microRNA array cards. I found that 8 miRNAs were deregulated in exosomes from EOC patients compared with healthy women. Four miRNAs (miR-21, miR-100, miR-200b and miR-320) were upregulated and the others (miR-16, miR-93, miR-126 and miR-223) were downregulated in exosomes from EOC patients. The levels of exosomal miR-23a and miR-92a were associated with benign ovarian tumors since their occurrence was significantly lower in ovarian cystadenoma patients than in the EOC group or healthy women. In addition, I detected higher plasma levels of exosomes in ovarian cystadenoma and EOC patients, in particular in FIGO IV patients, than in healthy women and FIGO III patients. The low levels of exosomes that I found in healthy women may be mainly derived from platelets, erythrocytes and endothelial cells, and have been shown to be important in common hemostatic events in normal physiology (50). The higher levels of exosomes in FIGO IV than in FIGO III patients detected in my study suggest that a higher release of exosomes correlates with their higher invasive potential. In line to my observations, Kobayashi et al. reported that high invasive ovarian cancer cells release significantly more exosomes than low invasive cells (51). This observation supports the assumption, that exosomes serve as an important mediator between tumor and its microenvironment and could increase cell invasion. Thus, they may help to form a pre-metastatic niche and prepare secondary sites for metastasis (52). Surprisingly, I also detected high plasma levels of exosomes in ovarian cystadenoma patients, suggesting that an excessive secretion of exosomes also occurs in these tumors reflecting extensive inflammatory processes that are not malignant.

Besides the increased secretion of exosomes, the selective packaging of miRNAs may contribute to the pathogenesis of ovarian tumors. As far as I know, I demonstrate for the first time sets of enriched miR-21, miR-100, miR-200b and miR-320 as well as of under-presented miR-16, miR-93, miR-126 and miR-223 in exosomes of EOC patients compared with those of healthy women. In my study, I found the highest fold increase in concentrations

of miR-200b in exosomes from EOC patients compared with those in exosomes of healthy women. The levels of this exosomal miRNA were about five times higher in EOC patients than in healthy women, and correlated with the tumor marker CA125 currently routinely used as screening parameter for EOC, as well as with poor overall survival. In comparison to the other exosomal miRNAs analyzed, miR-200b had also the highest sensitivity (64%) and specificity (86%) to discriminate EOC from healthy women. These data substantiate our previous findings also showing the positive relationship of exosomal miR-200b with CA125 values and its prognostic relevance in EOC patients (17). On the other hand, my in vitro experiments and confirmed previously reported data (53) showed that miR-200b acts rather as a tumor suppressor, inhibiting cell proliferation and promoting apoptosis of ovarian cancer cells. However, miR-200 family members seem to be versatile players (54). They play a major role in the suppression of EMT and metastasis (55, 56), and low-level expression of miR-200 members in advanced ovarian tumors significantly correlate with cancer recurrence and poor overall survival, whereas overexpression of miR-200b inhibit ovarian cancer cell migration (53). Moreover, other studies have shown that its elevated expression is a significant characteristic of EOC tissue and serum (57-59). Using microarray analysis, it was reported that the levels of miR-200b derived from EpCAM-positive exosomes were higher in EOC patients than in patients with benign ovarian diseases. These findings demonstrate the dual character of miR-200b. In particular, my data suggest that in vitro miR-200b acts as a tumor suppressor in suppressing cell proliferation and promoting apoptosis, and in vivo, miR-200b selectively packaged in exosomes serves as a diagnostic and prognostic oncomiR.

MiR-320 has been reported also to have a dual character. A study showed by building a miRNA model that in EOC, the high expression of miR-320 is associated with negative prognosis, migration and invasion of cancer and high risk of metastasis (60). In contrast, another study revealed that miR-320 is rather a tumor suppressor due to its downregulation in EOC tissue compared with non-tumor tissue, and its ability to suppress cell proliferation, cycle and invasion through targeting Twist homolog 1 (TWIST1) in EOC (61). Some other studies show that miR-320 can also act as tumor suppressor in other gynecological cancers

such as breast cancer and cervical cancer (62, 63). It was also reported that miR-320 inhibits invasion and induces apoptosis in gastric cancer cells (64). In my study, I found that miR-320 is preferentially packaged in exosomes of EOC patients, but has no impact on cell proliferation and apoptosis in ovarian cancer cells.

MiR-100 can exert both tumor suppressor and oncogenic functions in various cancer types, too. However, in EOC, miR-100 seems to be a tumor suppressor, since its levels are usually lower in EOC tissues than in adjacent normal tissues (65), and correlate with progression and poor prognosis of EOC (66). Upregulation of miR-100 can inhibit cell proliferation, promote cell apoptosis and cell cycle arrest, and sensitize resistant EOC cells to cisplatin, resulting in reversing drug resistance (67). Overexpression of miR-100 can also enhance the sensitivity to rapamycin in clear cell ovarian cancer (68). In serous ovarian carcinoma, miR-320 is down-regulated compared with normal ovarian tissues (69). In my present study, I show that the levels of miR-100 are two times higher in exosomes from EOC patients compared with those in healthy women, indicating a selective packaging process and a potential occurrence of exosomes whose cargo also contains tumor suppressive potential.

MiR-21 is one of the best studied miRNAs, is overexpressed in most cancer types and thus, displays oncogenic activity. MiR-21 participates in the occurrence and development of gastric adenocarcinoma (70). MiR-21 is found over-expressed in malignant pleural mesothelioma compared to normal mesothelium (71). Other findings show that miR-21 functions as a tumor facilitator in lung adenocarcinoma through targeting HMG box transcription factor 1 (72). Accumulating evidence supports a central role for miR-21 in ovarian cancer initiation, progression, and chemoresistance (41, 73-76). Here, I show that high amounts of miR-21 are also packaged in exosomes of EOC patients.

MiR-93 was described to be a potential suppressor of ovarian cell proliferation and to inhibit EOC tumorigenesis and progression by targeting the small G protein/guanosine triphosphatase RhoC (Ras homolog gene family member C) (77). Besides, miR-93 can also promote epithelial-mesenchymal transition of endometrial carcinoma cells (78). In serous ovarian carcinoma, miR-93 is down-regulated compared with ovarian normal tissues (79, 80).

A further research study found that miR-93 is related to chemoresistance in ovarian cancer cells (81). MiR-126 is a tumor suppressor not only in EOC, and decreases serine/threonine p21-activated kinase 4 expression to inhibit invasive growth of EOC cells (82), but also in gastric cancer (83) and non-small-cell lung cancer (84). In line with their tumor suppressive behavior, my quantitative analyses show an approximatively twice lower presence of miR-93 and miR-126 in exosomes from EOC patients than in healthy women. Aberrant miR-223 expression has been implicated in the pathogenesis of a wide range of cancers. In EOC, miR-223 seems to serve as an oncomiR (85), since some studies found that miR-223 is up-regulated in ovarian cancer tissues compared with normal ovarian tissues (86, 87). However, I found a downregulation of this miRNA in exosomes from EOC patients compared with healthy women, thus a decrease in its oncogenic potential in exosomes from EOC patients. Alike, Huang et al. showed a significant overexpression of miR-223 in serum from esophageal squamous cell carcinoma (ESCC) patients compared with normal controls, but similar levels in exosomes from ESCC patients and normal controls (88).

The first direct evidence of miRNAs playing a role in human cancer came from Calin et al. in 2002. They demonstrated that the miRNA cluster containing miR-16 was deleted in a significant portion of chronic lymphocytic leukemia cases (89). To date, miR-16 has been used as a reference miRNAs for data normalization due to its steadily high expression, and conversely, has been reported to act as tumor suppressor or oncomiR in different cancer types, thus to be involved in tumorigenicity both in vitro and in vivo (41, 90-93). MiR-16 expression may also be a potential therapeutic target and clinical biomarker of bone metastasis, because it is elevated in osteoclast differentiation and bone metastasis (94). In my present study, I found that only low amounts of miR-16 were packaged in exosomes from EOC patients, while another study showed that the serum levels of circulating miR-16 were neither up- nor downregulated in EOC patients compared with healthy women (16).

Finally, my analyses show lower levels of exosomal miR-23a and miR-92a in ovarian cystadenoma patients than in healthy women. No deregulation of miR-23a could be observed in exosomes from EOC patients, but a downregulation of miR-92a only in serous

EOC patients and not in patients harboring a different histology. My findings point to a role of these miRNAs in benign ovarian tumors, in particular of miR-23a. A recent study by Xiong et al. also showed that the levels of serum miR-23a were significantly lower in women with polycystic ovary syndrome (PCOS) than healthy women. The likelihood of women with PCOS decreased by 0.01-fold for every one fold increase in miR-23a expression (95). Otherwise, miR-23a is also found as an oncogene contributing to the malignancy of EOC cells (96). Moreover, miR-23a is related with chemoresistance in ovarian cancer (97).

In conclusion, my findings suggest a specific miRNA pattern in exosomes from EOC and ovarian cystadenoma patients. The frequent dual character of miRNAs in tumor cells is accompanied by the enrichment of oncogenic and tumor suppressive miRNAs in exosomes that participate in cell-to-cell communication. Overall, exosomal miRNAs have potential relevance to be tumor markers in EOC. My findings show that exosomal miR-200b plays an important role in EOC. It is enriched in exosomes but inhibits cell proliferation and promotes apoptosis. Therefore, still a lot of work needs to do to reveal this complex regulatory network that maintains EOC development and progression.

5. Summary

Examination of deregulated levels of miRNAs and their characterization extend the understanding of carcinogenesis and provide new aspects of the complex regulation of gene expression. Exosomes also play an essential role in EOC because they are considered as mediators of intercellular communication and pathological processes, such as tumor development and progression. Specific miRNAs are packaged in exosomes that regulate processes to maintain tumor development and progression. In my study, I identified exosomal miRNAs that reflect the pathogenesis of epithelial ovarian cancer (EOC). MiRNA expression profiles were determined in exosomes derived from plasma of 106 EOC patients, 8 ovarian cystadenoma patients and 29 healthy women by a quantitative TaqMan real-time PCR-based microarray containing 48 different miRNAs. Identification of exosomes was performed by Western blot. Cell culture experiments were carried out to determine the impact of miR-200b and miR-320 on proliferation and apoptosis of the ovarian cancer cell lines SKOV3 and OVCAR3. The results of my study show that the levels of miR-21, miR-100, miR-200b and miR-320 were higher, whereas the levels of miR-16, miR-93, miR-126 and miR-223 were lower in exosomes from plasma of EOC patients than from healthy women. The levels of exosomal miR-23a and miR-92a were lower in ovarian cystadenoma patients than in EOC patients and healthy women, respectively. The levels of exosomal miR-21 and miR-200b could best discriminate between EOC patients and healthy women with a sensitivity of 61% and 64% and a specificity of 82% and 86%, respectively. The exosomal amounts of miR-200b correlated with the tumor marker CA125 and patient overall survival. Due to the functional analyses, miR-200b influenced cell proliferation and apoptosis in OVCAR3 cells. In summary, my study shows the diagnostic value and prognostic value of exosomal miRNAs and indicate a role of these miRNAs in the pathogenesis of EOC.

Zusammenfassung

Die Untersuchung von deregulierten Niveaus von miRNAs und deren Charakterisierung erweitern das Verständnis der Karzinogenese und liefern neue Aspekte der komplexen Regulation der Genexpression. Exosomen spielen auch eine wesentliche Rolle in EOC, da sie als Mediatoren interzellulärer Kommunikation und pathologischer Prozesse, wie der Tumorentwicklung und -progression, angesehen werden. Spezifische miRNAs werden in Exosomen verpackt, die Prozesse regulieren, um die Tumorentwicklung und Progression zu unterstützen. In meiner Studie identifizierte ich exosomale miRNAs, die die Pathogenese von epithelialem Ovarialkarzinom (EOC) widerspiegeln. MiRNA-Expressionsprofile wurden in Exosomen bestimmt, die aus Plasma von 106 EOC-Patientinnen, 8 Ovarialzystadenom-Patientinnen und 29 gesunden Frauen durch einen quantitativen TaqMan real-time PCR-basierten Microarray mit 48 verschiedenen miRNAs isoliert wurden. Die Identifizierung von Exosomen erfolgte durch einen Western-Blot. Zellkulturexperimente wurden durchgeführt, um den Einfluss von miR-200b und miR-320 auf die Proliferation und Apoptose der Ovarialkarzinom-Zelllinien SKOV3 und OVCAR3 zu bestimmen. Die Ergebnisse meiner Studie zeigen, dass die Niveaus von miR-21, miR-100, miR-200b und miR-320 höher waren, während die Niveaus von miR-16, miR-93, miR-126 und miR-223 waren niedriger in Exosomen aus Plasma von EOC-Patientinnen als von gesunden Frauen. Die Spiegel von exosomalen miR-23a und miR-92a waren bei Ovarialzystadenom-Patientinnen niedriger als bei EOC Patientinnen und gesunden Frauen. Die Spiegel von exosomalen miR-21 und miR-200b konnten am besten zwischen EOC-Patienten und gesunden Frauen mit einer Sensitivität von 61% bzw. 64% und einer Spezifität von 82% bzw. 86% unterscheiden. Die exosomalen Konzentrationen von miR-200b korrelierten mit dem Tumormarker CA125 und dem Gesamtüberleben der Patientinnen. Gemäß den Funktionsanalysen beeinflusste miR-200b die Zellproliferation und Apoptose in OVCAR3-Zellen. Zusammengefasst zeigt meine Studie den diagnostischen und prognostischen Wert von exosomalen miRNAs beim Ovarialkarzinom.

6. References

1.   Jayson GC, Kohn EC, Kitchener HC, Ledermann JA. Ovarian cancer. Lancet. 2014;384(9951):1376-88.

2.   Longo DL. Harrison's principles of internal medicine. 18th ed. New York: McGraw-Hill; 2012.

3.   O'Leary B, Treacy T, Geoghegan T, Walsh T, Boyd B, Brennan D. Incidental Thoracic Findings on Routine Computed Tomography in Epithelial Ovarian Cancer. Int J Gynecol Cancer. 2017;27:1614-.

4.   Phelan CM, Kuchenbaecker KB, Tyrer JP, Kar SP, Lawrenson K, Winham SJ, et al. Identification of 12 new susceptibility loci for different histotypes of epithelial ovarian cancer. Nature genetics. 2017;49(5):680-91.

5.   Vaughan S, Coward JI, Bast RC, Jr., Berchuck A, Berek JS, Brenton JD, et al. Rethinking ovarian cancer: recommendations for improving outcomes. Nature reviews Cancer. 2011;11(10):719-25.

6.   Jones PM, Drapkin R. Modeling High-Grade Serous Carcinoma: How Converging Insights into Pathogenesis and Genetics are Driving Better Experimental Platforms. Front Oncol. 2013;3:217.

7.   Prat J. Ovarian carcinomas: five distinct diseases with different origins, genetic alterations, and clinicopathological features. Virchows Archiv : an international journal of pathology. 2012;460(3):237-49.

8.   Langyel E. Ovarian Cancer Development and Metastasis. Am J Pathol. 2010;177(3):1053-64.

9.   Munoz-Casares FC, Rufian S, Arjona-Sanchez A, Rubio MJ, Diaz R, Casado A, et al. Neoadjuvant intraperitoneal chemotherapy with paclitaxel for the radical surgical treatment of peritoneal carcinomatosis in ovarian cancer: a prospective pilot study. Cancer chemotherapy and pharmacology. 2011;68(1):267-74.

10.   Hoffman BL. Williams gynecology. Third edition. ed. New York: McGraw-Hill Education; 2016. xxv, 1270 pages p.

11.   Moghaddam SM, Amini A, Morris DL, Pourgholami MH. Significance of vascular endothelial growth factor in growth and peritoneal dissemination of ovarian cancer. Cancer Metast Rev. 2012;31(1-2):143-62.

12.   Kobel M, Kalloger SE, Boyd N, McKinney S, Mehl E, Palmer C, et al. Ovarian carcinoma subtypes are different diseases: implications for biomarker studies. PLoS medicine. 2008;5(12):e232.

13.   Burki TK. CA-125 blood test in early detection of ovarian cancer. Lancet Oncology. 2015;16(6):E269-E.

14.   Menon U, Griffin M, Gentry-Maharaj A. Ovarian cancer screening-Current status, future directions. Gynecologic Oncology. 2014;132(2):490-5.

15.   Santillan A, Garg R, Zahurak ML, Gardner GJ, Giuntoli RL, Armstrong DK, et al. Risk of epithelial ovarian cancer recurrence in patients with rising serum CA-125 levels within the normal range. J Clin Oncol. 2005;23(36):9338-43.

16.   Meng X, Joosse SA, Muller V, Trillsch F, Milde-Langosch K, Mahner S, et al. Diagnostic and prognostic potential of serum miR-7, miR-16, miR-25, miR-93, miR-182, miR-376a and miR-429 in ovarian cancer patients. Br J Cancer. 2015;113(9):1358-66.

17.   Meng X, Muller V, Milde-Langosch K, Trillsch F, Pantel K, Schwarzenbach H. Diagnostic and prognostic relevance of circulating exosomal miR-373, miR-200a, miR-200b and miR-200c in patients with epithelial ovarian cancer. Oncotarget. 2016;7(13):16923-35.

18.   Zhang R, Pu W, Zhang S, Chen L, Zhu W, Xiao L, et al. Clinical value of ALU concentration and integrity index for the early diagnosis of ovarian cancer: A retrospective cohort trial. PloS one. 2018;13(2):e0191756.

19.   Jacobs IJ, Menon U, Ryan A, Gentry-Maharaj A, Burnell M, Kalsi JK, et al. Ovarian cancer screening and mortality in the UK Collaborative Trial of Ovarian Cancer Screening (UKCTOCS): a randomised controlled trial. Lancet. 2016;387(10022):945-56.

20.   Cortez AJ, Tudrej P, Kujawa KA, Lisowska KM. Advances in ovarian cancer therapy. Cancer chemotherapy and pharmacology. 2018;81(1):17-38.

21.   du Bois A, Kristensen G, Ray-Coquard I, Reuss A, Pignata S, Colombo N, et al. Standard first-line chemotherapy with or without nintedanib for advanced ovarian cancer (AGO-OVAR 12): a randomised, double-blind, placebo-controlled phase 3 trial. The Lancet Oncology. 2016;17(1):78-89.

22.   Coleman RL, Oza AM, Lorusso D, Aghajanian C, Oaknin A, Dean A, et al. Rucaparib maintenance treatment for recurrent ovarian carcinoma after response to platinum therapy (ARIEL3): a randomised, double-blind, placebo-controlled, phase 3 trial. Lancet. 2017;390(10106):1949-61.

23.   Zahra F. Pattern of benign ovarian cysts in Qatari women. Qatar Med J. 2016;2016(2):17.

24.   Jung SE, Lee JM, Rha SE, Byun JY, Jung JI, Hahn ST. CT and MR imaging of ovarian tumors with emphasis on differential diagnosis. Radiographics. 2002;22(6):1305-25.

25.   Brown J, Frumovitz M. Mucinous tumors of the ovary: current thoughts on diagnosis and management. Curr Oncol Rep. 2014;16(6):389.

26.   Cevik M, Guldur ME. An Extra-large Ovarian Mucinous Cystadenoma in a Premenarchal Girl and a Review of the Literature. J Pediatr Adol Gynec. 2013;26(1):22-6.

27.   Fajau-Prevot C, Le Gac YT, Chevreau C, Cohade C, Gatimel N, Parinaud J, et al. Ovarian Mucinous Cystadenoma After Ovarian Graft. Obstet Gynecol. 2017;129(6):1035-6.

28.   Cho SM, Byun JY, Rha SE, Jung SE, Park GS, Kim BK, et al. CT and MRI findings of cystadenofibromas of the ovary. Eur Radiol. 2004;14(5):798-804.

29.   Roth LM. Recent advances in the pathology and classification of ovarian sex cord-stromal tumors. Int J Gynecol Pathol. 2006;25(3):199-215.

30.   Simpson RJ, Lim JW, Moritz RL, Mathivanan S. Exosomes: proteomic insights and diagnostic potential. Expert review of proteomics. 2009;6(3):267-83.

31.   Colletti M, Petretto A, Galardi A, Di Paolo V, Tomao L, Lavarello C, et al. Proteomic Analysis of Neuroblastoma-Derived Exosomes: New Insights into a Metastatic Signature. Proteomics. 2017;17(23-24).

32.   Kowal J, Arras G, Colombo M, Jouve M, Morath JP, Primdal-Bengtson B, et al. Proteomic comparison defines novel markers to characterize heterogeneous populations of extracellular vesicle subtypes. Proceedings of the National Academy of Sciences of the United States of America. 2016;113(8):E968-77.

33.   Arenaccio C, Federico M. The Multifaceted Functions of Exosomes in Health and Disease: An Overview. Advances in experimental medicine and biology. 2017;998:3-19.

34.   Schwarzenbach H. The clinical relevance of circulating, exosomal miRNAs as biomarkers for cancer. Expert Rev Mol Diagn. 2015;15(9):1159-69.

35.   Shao YK, Shen YW, Chen T, Xu F, Chen XW, Zheng S. The functions and clinical applications of tumor-derived exosomes. Oncotarget. 2016;7(37):60736-51.

36.   Azmi AS, Bao B, Sarkar FH. Exosomes in cancer development, metastasis, and drug resistance: a comprehensive review. Cancer metastasis reviews. 2013;32(3-4):623-42.

37.   Li SP, Lin ZX, Jiang XY, Yu XY. Exosomal cargo-loading and synthetic exosome-mimics as potential therapeutic tools. Acta pharmacologica Sinica. 2018.

38.   Valadi H, Ekstrom K, Bossios A, Sjostrand M, Lee JJ, Lotvall JO. Exosome-mediated transfer of mRNAs and microRNAs is a novel mechanism of genetic exchange between cells. Nature cell biology. 2007;9(6):654-9.

39.   Chen X, Liang H, Zhang J, Zen K, Zhang CY. Horizontal transfer of microRNAs: molecular mechanisms and clinical applications. Protein & cell. 2012;3(1):28-37.

40.   Pant S, Hilton H, Burczynski ME. The multifaceted exosome: biogenesis, role in normal and aberrant cellular function, and frontiers for pharmacological and biomarker opportunities. Biochemical pharmacology. 2012;83(11):1484-94.

41.   Schwarzenbach H, Nishida N, Calin GA, Pantel K. Clinical relevance of circulating cell-free microRNAs in cancer. Nat Rev Clin Oncol. 2014;11(3):145-56.

42.   Kong YW, Ferland-McCollough D, Jackson TJ, Bushell M. microRNAs in cancer management. The Lancet Oncology. 2012;13(6):e249-58.

43. Schwarzenbach H. Diagnostic relevance of circulating cell-free and exosomal microRNAs and long non-coding RNAs in blood of cancer patients. Laboratoriumsmedizin. 2016;40(5):345-53.

44. Schwarzenbach H. Clinical Relevance of Circulating, Cell-Free and Exosomal microRNAs in Plasma and Serum of Breast Cancer Patients. Oncol Res Treat. 2017;40(7-8):423-9.

45. Krol J, Loedige I, Filipowicz W. The widespread regulation of microRNA biogenesis, function and decay. Nat Rev Genet. 2010;11(9):597-610.

46. Cortez MA, Bueso-Ramos C, Ferdin J, Lopez-Berestein G, Sood AK, Calin GA. MicroRNAs in body fluids-the mix of hormones and biomarkers. Nature Reviews Clinical Oncology. 2011;8(8):467-77.

47. Cheng AM, Byrom MW, Shelton J, Ford LP. Antisense inhibition of human miRNAs and indications for an involvement of miRNA in cell growth and apoptosis. Nucleic acids research. 2005;33(4):1290-7.

48. Meng X, Muller V, Milde-Langosch K, Trillsch F, Pantel K, Schwarzenbach H. Circulating Cell-Free miR-373, miR-200a, miR-200b and miR-200c in Patients with Epithelial Ovarian Cancer. Advances in experimental medicine and biology. 2016;924:3-8.

49. Jensen EC. The basics of western blotting. Anatomical record. 2012;295(3):369-71.

50. Yuana Y, Sturk A, Nieuwland R. Extracellular vesicles in physiological and pathological conditions. Blood Rev. 2013;27(1):31-9.

51. Kobayashi M, Salomon C, Tapia J, Illanes SE, Mitchell MD, Rice GE. Ovarian cancer cell invasiveness is associated with discordant exosomal sequestration of Let-7 miRNA and miR-200. J Transl Med. 2014;12:4.

52. Steinbichler TB, Dudas J, Riechelmann H, Skvortsova, II. The role of exosomes in cancer metastasis. Semin Cancer Biol. 2017;44:170-81.

53. Zuberi M, Mir R, Das J, Ahmad I, Javid J, Yadav P, et al. Expression of serum miR-200a, miR-200b, and miR-200c as candidate biomarkers in epithelial ovarian cancer and their association with clinicopathological features. Clin Transl Oncol. 2015;17(10):779-87.

54.	Muralidhar GG, Barbolina MV. The miR-200 Family: Versatile Players in Epithelial Ovarian Cancer. Int J Mol Sci. 2015;16(8):16833-47.

55.	Burk U, Schubert J, Wellner U, Schmalhofer O, Vincan E, Spaderna S, et al. A reciprocal repression between ZEB1 and members of the miR-200 family promotes EMT and invasion in cancer cells. EMBO Rep. 2008;9(6):582-9.

56.	Koutsaki M, Spandidos DA, Zaravinos A. Epithelial-mesenchymal transition-associated miRNAs in ovarian carcinoma, with highlight on the miR-200 family: prognostic value and prospective role in ovarian cancer therapeutics. Cancer Lett. 2014;351(2):173-81.

57.	Kan CW, Hahn MA, Gard GB, Maidens J, Huh JY, Marsh DJ, et al. Elevated levels of circulating microRNA-200 family members correlate with serous epithelial ovarian cancer. BMC Cancer. 2012;12:627.

58.	Liu XG, Zhu WY, Huang YY, Ma LN, Zhou SQ, Wang YK, et al. High expression of serum miR-21 and tumor miR-200c associated with poor prognosis in patients with lung cancer. Med Oncol. 2012;29(2):618-26.

59.	Pendlebury A, Hannan NJ, Binder N, Beard S, McGauran M, Grant P, et al. The circulating microRNA-200 family in whole blood are potential biomarkers for high-grade serous epithelial ovarian cancer. Biomed Rep. 2017;6(3):319-22.

60.	Wang W, Yang J, Xiang YY, Pi J, Bian J. Overexpression of Hsa-miR-320 Is Associated With Invasion and Metastasis of Ovarian Cancer. J Cell Biochem. 2017;118(11):3654-61.

61.	Li C, Duan P, Wang J, Lu X, Cheng J. miR-320 inhibited ovarian cancer oncogenicity via targeting TWIST1 expression. Am J Transl Res. 2017;9(8):3705-13.

62.	Bai JW, Wang X, Zhang YF, Yao GD, Liu H. MicroRNA-320 inhibits cell proliferation and invasion in breast cancer cells by targeting SOX4. Oncology Letters. 2017;14(6):7145-52.

63.	Shi C, Zhang ZY. MicroRNA-320 suppresses cervical cancer cell viability, migration and invasion via directly targeting FOXM1. Oncology Letters. 2017;14(3):3809-16.

64.   Zhao Y, Dong QZ, Wang EH. MicroRNA-320 inhibits invasion and induces apoptosis by targeting CRKL and inhibiting ERK and AKT signaling in gastric cancer cells. Oncotargets Ther. 2017;10:1049-58.

65.   Peng DX, Luo M, Qiu LW, He YL, Wang XF. Prognostic implications of microRNA-100 and its functional roles in human epithelial ovarian cancer. Oncol Rep. 2012;27(4):1238-44.

66.   Azizmohammadi S, Azizmohammadi S, Safari A, Kosari N, Kaghazian M, Yahaghi E, et al. The role and expression of miR-100 and miR-203 profile as prognostic markers in epithelial ovarian cancer. Am J Transl Res. 2016;8(5):2403-10.

67.   Guo P, Xiong X, Zhang S, Peng D. miR-100 resensitizes resistant epithelial ovarian cancer to cisplatin. Oncol Rep. 2016;36(6):3552-8.

68.   Nagaraja AK, Creighton CJ, Yu ZF, Zhu HF, Gunaratne PH, Reid JG, et al. A Link between mir-100 and FRAP1/mTOR in Clear Cell Ovarian Cancer. Mol Endocrinol. 2010;24(2):447-63.

69.   Nam EJ, Yoon H, Kim SW, Kim H, Kim YT, Kim JH, et al. MicroRNA expression profiles in serous ovarian carcinoma. Clin Cancer Res. 2008;14(9):2690-5.

70.   Gu JB, Bao XB, Ma Z. Effects of miR-21 on proliferation and apoptosis in human gastric adenocarcinoma cells. Oncol Lett. 2018;15(1):618-22.

71.   Nicole L, Cappellesso R, Sanavia T, Guzzardo V, Fassina A. MiR-21 over-expression and Programmed Cell Death 4 down-regulation features malignant pleural mesothelioma. Oncotarget. 2018;9(25):17300-8.

72.   Su C, Cheng X, Li Y, Han Y, Song X, Yu D, et al. MiR-21 improves invasion and migration of drug-resistant lung adenocarcinoma cancer cell and transformation of EMT through targeting HBP1. Cancer Med. 2018.

73.   Baez-Vega PM, Echevarria Vargas IM, Valiyeva F, Encarnacion-Rosado J, Roman A, Flores J, et al. Targeting miR-21-3p inhibits proliferation and invasion of ovarian cancer cells. Oncotarget. 2016;7(24):36321-37.

74.   Pink RC, Samuel P, Massa D, Caley DP, Brooks SA, Carter DR. The passenger strand, miR-21-3p, plays a role in mediating cisplatin resistance in ovarian cancer cells. Gynecol Oncol. 2015;137(1):143-51.

75.   Chan JK, Blansit K, Kiet T, Sherman A, Wong G, Earle C, et al. The inhibition of miR-21 promotes apoptosis and chemosensitivity in ovarian cancer. Gynecol Oncol. 2014;132(3):739-44.

76.   Lou Y, Cui Z, Wang F, Yang X, Qian J. miR-21 down-regulation promotes apoptosis and inhibits invasion and migration abilities of OVCAR3 cells. Clin Invest Med. 2011;34(5):E281.

77.   Chen X, Chen S, Xiu YL, Sun KX, Zong ZH, Zhao Y. RhoC is a major target of microRNA-93-5P in epithelial ovarian carcinoma tumorigenesis and progression. Mol Cancer. 2015;14:31.

78.   Chen S, Chen X, Sun KX, Xiu YL, Liu BL, Feng MX, et al. MicroRNA-93 Promotes Epithelial-Mesenchymal Transition of Endometrial Carcinoma Cells. PloS one. 2016;11(11):e0165776.

79.   Wang L, Wang B, Fang M, Guo E, Cui M. Identification of microRNAs and target genes involved in serous ovarian carcinoma and their influence on survival. Eur J Gynaecol Oncol. 2014;35(6):655-61.

80.   Theriault BL, Basavarajappa HD, Lim H, Pajovic S, Gallie BL, Corson TW. Transcriptional and Epigenetic Regulation of KIF14 Overexpression in Ovarian Cancer. PloS one. 2014;9(3).

81.   Fu X, Tian J, Zhang L, Chen Y, Hao Q. Involvement of microRNA-93, a new regulator of PTEN/Akt signaling pathway, in regulation of chemotherapeutic drug cisplatin chemosensitivity in ovarian cancer cells. Febs Lett. 2012;586(9):1279-86.

82.   Luo P, Fei J, Zhou J, Zhang W. microRNA-126 suppresses PAK4 expression in ovarian cancer SKOV3 cells. Oncol Lett. 2015;9(5):2225-9.

83.   Feng RH, Chen XH, Yu YY, Su LP, Yu BQ, Li JF, et al. miR-126 functions as a tumour suppressor in human gastric cancer. Cancer Letters. 2010;298(1):50-63.

84. Grimolizzi F, Monaco F, Leoni F, Bracci M, Staffolani S, Bersaglieri C, et al. Exosomal miR-126 as a circulating biomarker in non-small-cell lung cancer regulating cancer progression. Sci Rep-Uk. 2017;7.

85. Haneklaus M, Gerlic M, O'Neill LA, Masters SL. miR-223: infection, inflammation and cancer. J Intern Med. 2013;274(3):215-26.

86. Fang G, Liu J, Wang QN, Huang XG, Yang RW, Pang YZ, et al. MicroRNA-223-3p Regulates Ovarian Cancer Cell Proliferation and Invasion by Targeting SOX11 Expression. International Journal of Molecular Sciences. 2017;18(6).

87. Arts FA, Keogh L, Smyth P, O'Toole S, Ta R, Gleeson N, et al. miR-223 potentially targets SWI/SNF complex protein SMARCD1 in atypical proliferative serous tumor and high-grade ovarian serous carcinoma. Hum Pathol. 2017;70:98-104.

88. Huang Z, Zhang L, Zhu D, Shan X, Zhou X, Qi LW, et al. A novel serum microRNA signature to screen esophageal squamous cell carcinoma. Cancer Med. 2017;6(1):109-19.

89. Calin GA, Dumitru CD, Shimizu M, Bichi R, Zupo S, Noch E, et al. Frequent deletions and down-regulation of micro- RNA genes miR15 and miR16 at 13q14 in chronic lymphocytic leukemia. Proceedings of the National Academy of Sciences of the United States of America. 2002;99(24):15524-9.

90. Schwarzenbach H. Clinical significance of miR-15 and miR-16 in ovarian cancer. Transl Cancer Res. 2016;5:S50-S3.

91. Stuckrath I, Rack B, Janni W, Jager B, Pantel K, Schwarzenbach H. Aberrant plasma levels of circulating miR-16, miR-107, miR-130a and miR-146a are associated with lymph node metastasis and receptor status of breast cancer patients. Oncotarget. 2015;6(15):13387-401.

92. Huang E, Liu R, Chu Y. miRNA-15a/16: as tumor suppressors and more. Future Oncol. 2015;11(16):2351-63.

93. Han S, Wang D, Tang GH, Yang XX, Jiao CY, Yang RJ, et al. Suppression of miR-16 promotes tumor growth and metastasis through reversely regulating YAP1 in human cholangiocarcinoma. Oncotarget. 2017;8(34):56635-50.

94.   Ell B, Mercatali L, Ibrahim T, Campbell N, Schwarzenbach H, Pantel K, et al. Tumor-induced osteoclast miRNA changes as regulators and biomarkers of osteolytic bone metastasis. Cancer Cell. 2013;24(4):542-56.

95.   Xiong WX, Lin Y, Xu LL, Tamadon A, Zou S, Tian FB, et al. Circulatory microRNA 23a and microRNA 23b and polycystic ovary syndrome (PCOS): the effects of body mass index and sex hormones in an Eastern Han Chinese population. J Ovarian Res. 2017;10.

96.   Yang Z, Wang XL, Bai R, Liu WY, Li X, Liu M, et al. miR-23a promotes IKKalpha expression but suppresses ST7L expression to contribute to the malignancy of epithelial ovarian cancer cells. Br J Cancer. 2016;115(6):731-40.

97.   Jin AH, Wei ZL. Molecular mechanism of increased sensitivity of cisplatin to ovarian cancer by inhibition of microRNA-23a expression. Int J Clin Exp Med. 2015;8(8):13329-34.

7. List of abbreviations

%	Percent
°C	Celsius Degree
µl	Microliter
µm	Micrometer
AGO2	Argonaute-2
ANOVA	Analysis of Variance
ATCC	American Type Culture Collection
AUC	Area Under the Curve
BRCA	Breast Cancer
BSA	Bovine Serum Albumin
CA125	Carbohydrate Antigen 125
CCOC	Clear Cell Ovarian Cancer
cDNA	Complementary DNA
CO_2	Carbon Dioxide
Cq	Cycle of Quantification
DMSO	dimethylsulfoxide
DSMZ	Deutsche Sammlung von Mikroorganismen und Zellkulturen
EMT	epithelial-mesenchymal transition
ENOC	Endometrioid Ovarian cancer
EOC	Epithelial Ovarian Cancer
EpCAM	Epithelial Cell Adhesion Molecule
ESCC	Esophageal Squamous Cell Carcinoma
FACS	Fluorescence-activated Cell Sorting
FCS	Fetal Calf Serum
FIGO	International Federation of Gynecology and Obstetrics
FITC	Fluorescein Isothiocyanate
g	Gram
g	Gravity
G	Grading
H	Hour
H_2O_2	Hydrogen Peroxide
HCl	Hydrochloric Acid
HGSOC	High Grade Serous Ovarian Cancer
HRP	Horseradish peroxidase
kDa	kilo Daltons
LGEOS	low grade endometrioid ovarian carcinoma

LGSOC	Low Grade Serous Ovarian Cancer
M	Mole
MET	mesenchymal-epithelial transition
mg	Milligram
MgCl2	Magnesium chloride
min	Minute
miRNA	microRNA
ml	Milliliter
mM	Millimole
MMPs	matrix metalloproteinases
MOC	Mucinous Ovarian Cancer
MRI	Magnetic Resonance Imaging
mRNA	Message RNA
MTT	3-(4,5-dimethylthiazol-2-yl)-2,5-diphenyltetrazolium bromide
MVBs	multivesicular bodies
NCCN	National Comprehensive Cancer Network
nM	Nanomole
NP-40	nonyl phenoxypolyethoxylethanol
OD	Optical Density
ORF	open reading frame
OS	Overall Survival
PBS	Phosphate Buffered Saline
PCOS	Polycystic Ovary Syndrome
pH	potential of hydrogen
PI	Propidium Iodide
pre-miRNA	precursor miRNA
pri-miRNA	primary miRNA
PS	Phospholipid Phosphatidylserine
PVDF	Polyvinylidene Fluoride
RhoC	Ras homolog gene family member C
RIPA	Radioimmunoprecipitation Assay
RISC	miRNA-induced silencing complex
RNAPII	RNA polymerase II
ROC	Receiver Operating Characteristic
RPMI	Roswell Park Memorial Institute
RT	Room Temperature
RT-PCR	Reverse Transcription-Polymerase Chain Reaction

SDS-PAGE	Sodium dodecyl sulfate polyacrylamide gel electrophoresis
sec	Second
snRNU6	small nuclear ribonucleoprotein U6
TBST	Tris-Buffered Saline Tween
TRBP	tar-RNA binding protein
TWIST1	Twist homolog 1
UTR	Untranslated Region
V	Voltage
VEGF	vascular endothelial growth factor

8. Acknowledgement

9. Curriculum Vitae

Personal Information

Name: Pan, Chi

Date of Birth: 16/12/1990

Gender: Male

Nationality: Chinese

Email: panchiseu@gmail.com

Telephone: 0176 4760 5437

Educational Background

Oct, 2016: Start of MD study at University Medical Center Hamburg-Eppendorf,Hamburg, Germany

Sep, 2014-Jul, 2016: Master of Clinical Medicine, Southeast University, Nanjing, PR of China

Sep, 2009-Jul, 2014: Bachelor of Clinical Medicine, Southeast University, Nanjing, PR of

China

Awards and Honors

Scholarship from China Scholarship Council; China Scholarship Council, 2016.

Outstanding Cadre of editorial department in school of medicine; Southeast University, 2013;

Outstanding Director of editorial department in school of medicine, Southeast University, 2012;

Social work excellence award; Outstanding Director of campus student, Southeast University, 2011;

Dalian Dong Gang scholarships, Southeast University, 2010;

Academic Experience

Oct 23, 2017: Talk on "Circulating exosomal microRNAs in blood of epithelial ovarian cancer patients" at the seminar of the institute of Tumor biology, University Medical Center Hamburg-Eppendorf, Germany

Sep 2014-Jun 2016   Residency Training in Affiliated Zhongda Hospital, Southeast University, Nanjing, Jiangsu, China

Jun 2013- Jun 2014   Internship in Nanjing First Hospital, Affiliated Nanjing First Hospital, Nanjing Medical University, Nanjing, Jiangsu, China

Jul 2012- Aug 2012   Internship in Nanjing First Hospital, Affiliated Nanjing First Hospital, Nanjing Medical University, Nanjing, Jiangsu, China

10. Eidesstattliche Versicherung

Ich versichere ausdrücklich, dass ich die Arbeit selbständig und ohne fremde Hilfe verfasst, andere als die von mir angegebenen Quellen und Hilfsmittel nicht benutzt und die aus den benutzten Werken wörtlich oder inhaltlich entnommenen Stellen einzeln nach Ausgabe (Auflage und Jahr des Erscheinens), Band und Seite des benutzten Werkes kenntlich gemacht habe.
Ferner versichere ich, dass ich die Dissertation bisher nicht einem Fachvertreter an einer anderen Hochschule zur Überprüfung vorgelegt oder mich anderweitig um Zulassung zur Promotion beworben habe.
Ich erkläre mich einverstanden, dass meine Dissertation vom Dekanat der Medizinischen Fakultät mit einer gängigen Software zur Erkennung von Plagiaten überprüft werden kann.

Unterschrift: .... *Chi Pan* ....